J. Fluid Mech. (1987), *vol.* 180, *pp.* 231–266
Printed in Great Britain

Rough-wall turbulent boundary layers in the transition regime

By PROMODE R. BANDYOPADHYAY
Mail Stop 163, NASA Langley Research Center, Hampton, VA 23665–5225, USA

(Received 11 December 1985 and in revised form 13 November 1986)

This paper describes an experimental study of turbulent boundary layers over two-dimensional spanwise groove and three-dimensional sandgrain roughnesses in the 'transition regime' between hydraulically smooth and fully rough conditions. Mean-flow measurements show that a state of kinematic near-self-preservation is also reached by sandgrain roughness and not just by *d*-type grooved roughness alone as commonly believed; sandgrain roughness simply requires an order-of-magnitude-longer length to reach such a state. The two roughness Reynolds numbers demarcating the boundaries of the transition regime of *k*-type roughnesses are found to decrease with increasing roughness-element spanwise aspect ratio (span/height). A more important role of the upper-Reynolds-number limit of the transition regime in the drag behaviour is indicated. The two Reynolds-number limits of the transition regime correlate with the two critical Reynolds numbers that describe the stability of the vortex-shedding process existing behind a similar but isolated roughness element lying submerged in an otherwise laminar boundary layer. The results provide a guideline for reducing *k*-type rough-wall drag by lowering the spanwise aspect ratio of the roughness elements. The vortex-shedding process in rough-wall turbulent boundary layers is described by the stability parameter $U_\tau\,(\bar{T}/\nu)^{\frac{1}{2}}$ whose value is the same for all roughnesses examined herein; here U_τ is the friction velocity, $\bar{T}$ is the mean time period of vortex shedding and ν is the kinematic viscosity of the fluid.

1. Introduction

1.1. *Roughness function*

The effect of surface roughness on turbulent-boundary-layer characteristics is commonly expressed by the roughness function $\Delta U/U_\tau$. Hama (1954) showed that this function is related to the coefficient of local skin friction c_f through the following relationship:

$$\frac{\Delta U}{U_\tau} = \left(\frac{2}{c_f}\right)^{\frac{1}{2}}_{\text{smooth}} - \left(\frac{2}{c_f}\right)^{\frac{1}{2}}_{\text{rough}}, \tag{1}$$

where $c_f = \tau_w/\frac{1}{2}\rho U_\infty^2$, τ_w being the wall shear stress, ρ the fluid density, U_∞ the free-stream velocity and $U_\tau = (\tau_w/\rho)^{\frac{1}{2}}$. Equation (1) applies when the Reynolds number Re_{δ^*} is the same for the smooth and rough walls; here $Re_{\delta^*} = U_\infty \delta^*/\nu$, where δ^* is the displacement thickness and ν is the kinematic viscosity of the fluid. In other words, roughness function is a measure of the increase in local drag due to roughness. Earlier, Nikuradse (1933) had shown in a pipe flow that roughness leads to a downward shift in U/U_τ, where U is the local mean velocity (and hence the Δ introduced by Hama) of the logarithmic part of the velocity profile from the law of the wall for a smooth surface. However, instead of this downward shift in U/U_τ,

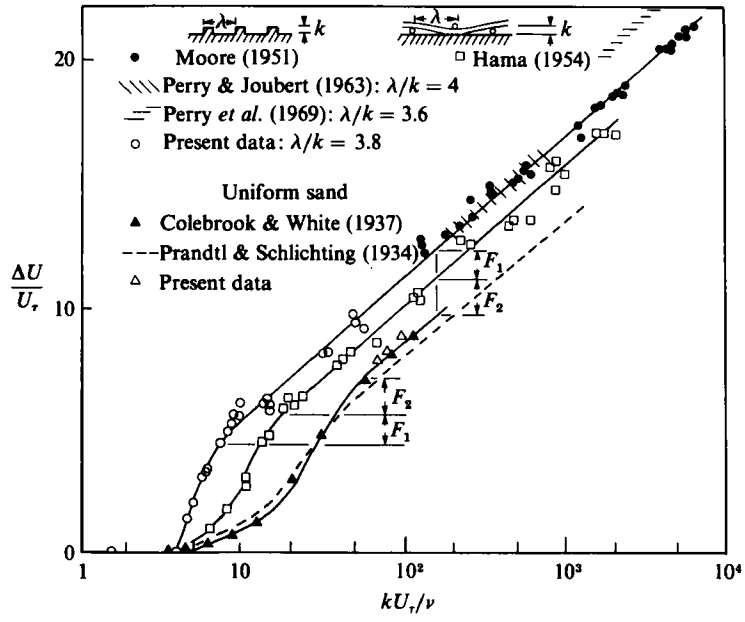

FIGURE 1. Roughness function in k-type roughness.

Nikuradse proposed a more involved measure (known as B) of the roughness effect and it appears to be Hama (1954) who first showed that the downward shift is in fact a physically more meaningful and simpler measure.

Figure 1 shows a portion of Hama's roughness-function data compilation. Three regimes can be discerned. These are generally termed hydraulically smooth, transitional and fully rough. The roughness-function behaviour is universal in the hydraulically smooth and fully rough regimes. However, in the transition regime, each roughness has its own characteristic behaviour. In 1956, Clauser noted, 'One of the challenging problems of current boundary layer research is to determine why these curves have the shapes they do and to predict the shape of the curve from the nature of the roughness elements'. Since that time, the transition regime has received only limited attention and the questions still remain unanswered.

The roughness function of the roughnesses in figure 1 depends on a Reynolds number based on the height of the roughness element k. For this reason, they have come to be known as k-type roughness (Perry, Schofield & Joubert 1969). However, experiments also show that (see Perry *et al.* 1969 for a review) the k-type scaling is not obeyed by a grooved roughness when the cavities are narrow ($w/k < 1$; figure 2). These are known as d-type roughness (discussed in §1.4). This paper deals largely with k-type roughness.

1.2. *Limits of the transition regime in k-type roughness*

Schlichting (1979) summarized the physical interpretation of the roughness regimes as follows. To be hydraulically smooth, the roughness elements must be submerged within the viscous sublayer. In the transition regime, the elements are only slightly thicker than the sublayer and their form drag is approximately equal to the increase in drag above the smooth-wall case. In the fully rough regime, the roughness elements are much larger than the sublayer thickness and most of the drag is roughness-element form drag.

The lower-Reynolds-number limit of the roughness transition regime $(U_\tau k/\nu)_\ell$ was studied by Prandtl & Schlichting (1934) and Goldstein (1936). (Here k is the height of the roughness element.) Based on the sand-roughened pipe-flow experiments of Nikuradse, the former authors observed that the surface is hydraulically smooth below a roughness Reynolds number Re_k $(= kU_\tau/\nu)$ of 7. A physical interpretation of this Reynolds number has been offered by Goldstein, who proposed that this represents the onset of a periodic vortex shedding behind the roughness elements. Goldstein's proposal for the turbulent flow is in fact an extension of an earlier work by Schiller (1932) who suggested that a laminar boundary layer remains hydraulically smooth till a roughness element starts shedding vortices. Schiller's suggestion is far reaching because it relates drag to vortex shedding. In the analyses of Schiller and Goldstein, $(U_\tau k/\nu)_\ell$ can be deduced if the critical Reynolds number Re_c for the onset of vortex shedding behind a single roughness element is known. Usually Re_c has been taken to be the same as its value for a circular cylinder in the free stream. In other words, it is implied that roughness wakes resemble a Kármán vortex street with a universal value of Re_c.

Whilst there is no data to suggest that Re_c depends on whether an obstacle is in the free stream or resting on the surface, the wall-proximity experiments of Furuya & Miyata (1972) reveal several differences in the wakes depending on what the aspect ratio of the obstacle is. For example, Re_c drops by more than half when the cylinder aspect ratio (l/d) increases from 1 to 6 (figure 25). Here l is the span and d is the diameter of the cylinder. Therefore, Re_c does not have a universal value. Furthermore, the wall proximity increases the Strouhal number for circular cylinders; at $Re = 40$, it is about 6 times that in the free stream. Here $Re = U_\infty d/\nu$. The latter observation led Furuya & Miyata to question if the very low-Reynolds-number wake is indeed a Kármán street.

There is another difference between the Kármán street in the free stream and the wake of a three-dimensional obstacle resting on the surface. In addition to the vortex loops, the latter contains the so-called necklace vortex which straddles the obstacle. Furuya & Miyata (1972) have observed that the necklace vortices are more stable than the periodically shed vortex loops. The necklace vortices have never been considered by any author to have any role in the rough-wall turbulent boundary layers. The experiments of Glotov & Korontsvit (1983) indicate that this may be justified. They showed that the upstream separation zone is substantially reduced when a small control needle is placed ahead of an obstacle resting on the surface. This suggests that one consequence of the interaction between the roughness elements is weaker necklace vortices. This aspect needs further investigation.

The upper critical roughness Reynolds number $(U_\tau k/\nu)_u$ demarcating the transition and fully rough regimes has not received any special attention. Rotta's (1950) analysis of Nikuradse's sand-roughened pipe-flow measurements indicate that, at an $U_\tau k/\nu$ of 55, there is no effective viscous sublayer. But, it is not known what happens to the above-mentioned unsteady wake at this Reynolds number.

1.3. *Transition regime in k-type roughness*

The transition regime has been studied experimentally by Colebrook & White (1937) and Hama (1954). The former authors studied sand-roughened pipes. The roughness function versus Reynolds number behaviour for uniform sand agreed well with that of Nikuradse (1933). Their experiments also show that, in the transition regime, the presence of only about 5 % of large grains in the roughness increases the roughness function substantially from the uniform-sand level. Such a non-uniform sand

roughness has a lower $(U_\tau k/\nu)_\ell$. A non-uniform-type roughness could also be produced if the roughness elements are 'sparsely' placed on a smooth surface. In the present study, such non-uniform types of roughness have not been considered.

Hama examined wire-mesh roughness. The roughness function for this surface is greater than that for sandgrain roughness and the critical Reynolds number $(U_\tau k/\nu)_u$ is lower. Hama's experiment clearly indicates that the upper limit of the transition regime, viz. $(U_\tau k/\nu)_u$, does not have a universal value. The frequently quoted value of $(U_\tau k/\nu)_u$ of 55 is valid for sandgrain roughness only. (Sometimes a limit of 70 (Schlichting 1979), instead of 55, is quoted. However, in view of Rotta's (1950) evaluation of Nikuradse's uniform-sand data a value of 55 is considered the result of a more refined analysis).

The concept of equivalent sand roughness, k_s is sometimes introduced in modelling. Schlichting (1936) defined k_s as the size of a sandgrain in Nikuradse's experiment that has the same resistance as the particular roughness being studied. Empirical forms of the resistance behaviour of sandgrain roughness in the transition regime has been given by Colebrook & White (1937) in terms of k_s. However, k_s is devoid of any physical significance and its determination is problematic. The roughness function in the transition regime has been formulated empirically also by Dvorak (1969) for several types of roughness.

1.4. *Roughness density*

In k-type roughness, attempts have been made (Bettermann 1965; Dvorak 1969; Simpson 1973) to express the roughness dependence of the roughness function versus $U_\tau k/\nu$ behaviour in terms of the roughness density. The approach covers the fully rough regime only where the roughness-function distribution is semilogarithmic irrespective of the type of roughness. Both Bettermann and Dvorak have defined the roughness density λ_s as the ratio of the total surface area to roughness area. They considered mainly the two-dimensional roughness normal to the flow where $\lambda_s = \lambda/s$ (figure 2). Note that, unlike l, λ is a streamwise and not a spanwise distance. Later on, Simpson considered a wider variety of roughness. He showed that the roughness-function variation correlates better if the roughness density (λ_k) is defined as the ratio of the total surface area to the total roughness frontal area normal to the flow. Thus, for two-dimensional roughness normal to the flow, $\lambda_k = \lambda/k$. Since k is related to form drag, its inclusion is more appropriate than s. In any case, Simpson's compilation of data shows that even λ_k does not collapse the various data to the two relationships of Bettermann and Dvorak. Systematic large variations between roughnesses can be discerned in the compilation and they can be described by Dvorak's relationship alone but with a variable slope. Thus, the definition of the roughness density λ_k is still inadequate and at least yet another unknown variable is involved. The present results show that this variable is l, the span of the roughness elements.

Perry *et al.* (1969) have shown that when a spanwise groove roughness consists of narrow cavities ($w/k < 1$; figure 2), in a zero pressure gradient, its roughness function does not depend on kU_τ/ν (unlike a wider cavity ($w/k > 1$) or sandgrain roughness); it depends on dU_τ/ν, where d is an outer-layer scale. Since the characteristic behaviour of a narrow cavity roughness was first detected in a pipe, such a roughness has come to be known as the d-type, where d stands for the pipe diameter.

Thus, there are two types of roughness, viz. d- and k-type. Perry *et al.*'s work clarifies one of the effects of roughness density. In the d-type, the cavity flow is more stable and it is not known why a large-scale length, viz. d or δ, is involved. (Here

δ is the boundary-layer thickness.) Nothing is known about the transition regime in a d-type roughness.

1.5. *Present work*

The distributions of roughness function in figure 1 show that, in a k-type roughness, compared with uniform sand, a wire-mesh roughness has a lower $(kU_\tau/\nu)_u$ and a higher $\Delta U/U_\tau$. Therefore, it can be suspected that $(kU_\tau/\nu)_u$ drops with increasing spanwise aspect ratio (λ_z) of the roughness elements. Here, λ_z is taken as the ratio of the span to height of the roughness elements (l/k, figure 2). In a distributed three-dimensional roughness, l is the largest spanwise lengthscale of the roughness elements in the (x, z)-plane. In a sandgrain λ_z is $O(1)$; in a square wire mesh, $\lambda_z > O(1)$, the side length of the square being l, and in a spanwise two-dimensional groove, $\lambda_z \gg O(1)$. Thus, a forest of thin tall needles ($\lambda_z \to 0$) and two-dimensional grooves ($\lambda_z \to \infty$) are the limiting types of roughness from the point of view of the spanwise aspect ratio. Figure 1 also shows that, in the fully rough regime where there is some available data, the k-type spanwise groove roughness has a higher roughness function than the wire mesh. Therefore, if the above dependence on aspect ratio is correct, the groove roughness should have the lowest $(kU_\tau/\nu)_u$ of all varieties of k-type roughness. The present study was initiated to see if this hypothesis of dependence of $(kU_\tau/\nu)_u$ on spanwise aspect ratio could be confirmed for k-type roughness.

In the following, an experimental investigation in k-type rough-wall turbulent boundary layers is described which examines the above-mentioned dependence of $(kU_\tau/\nu)_u$ on λ_z. Measurements, including vortex-shedding frequencies, have been made for two-dimensional spanwise groove and sandgrain roughness in the transition regime. These data have been examined for self-preserving behaviour and the correlation of $(kU_\tau/\nu)_u$ and $(kU_\tau/\nu)_\ell$ with the critical Reynolds numbers of the stability of the vortex-shedding process behind isolated roughness elements in a laminar boundary layer; in addition, the quasi-periodic vortex-shedding process behind a roughness element has been studied. Measurements have also been performed in a d-type grooved wall; its self-preservation and vortex-shedding characteristics have been compared with those of k-type walls.

2. Experiments

2.1. *Roughness*

Two roughness geometries have been tested, a two-dimensional roughness pattern and a sandgrain roughness. The roughness dimensions are given in table 1. Microphotographs of the roughnesses are available elsewhere (Bandyopadhyay 1986). For

Roughness	Material	k (mm)	w (mm)	s (mm)	l (cm)
d-type groove	Aluminium	0.33	0.23	0.30	28
k-type groove	Aluminium	0.31	0.94	0.23	28
Sandgrain	Aluminium oxide	0.56, 0.77 (50 and 36 grits respectively)	—	—	—

TABLE 1. Roughness dimensions

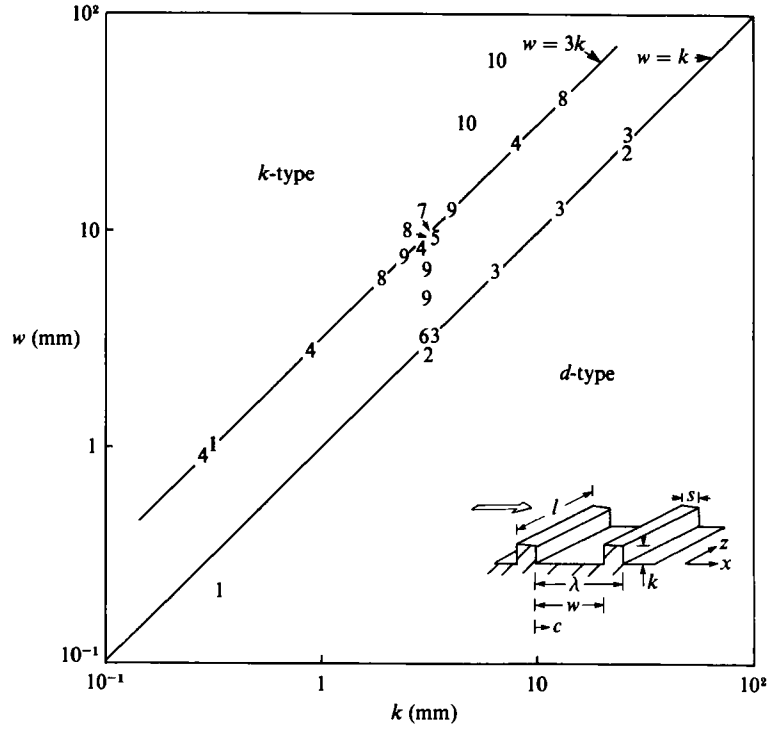

FIGURE 2. Groove geometries studied by various investigators: 1, present experiments; 2, Perry *et al.* (1969); 3, Townes & Sabersky (1966); 4, Hama (1954); 5, Antonia & Luxton (1971); 6, Osaka *et al.* (1982); 7, Perry & Joubert (1963); 8, Moore (1951); 9, Bettermann (1965); 10, Klein (1977).

the present experiments, the grooves have been machined out of 1.25 cm thick aluminium plates.

The groove geometry is defined in figure 2. The figure contains a summary of groove geometries studied by various investigators. Hama's (1954) wire mesh has been included for comparison. The present groove heights are the smallest examined thus far. It is clear that the grooves studied herein are also the ones most documented, viz. $w = k$ in the d-type and $w = 3k$ in the k-type. The ratio w/k could have an important effect on localized physics such as separation reattachment within the groove.

A cellular flow is likely to develop within a cavity when the incoming boundary layer is thin ($\delta/k < 1$). If δ is known, figure 2 can be utilized to determine whether the incoming boundary layer is relatively thick or thin. In the present experiments, the lowest δ/k is 35. Since this is large, the flow within the d-type grooves can be assumed to be two-dimensional and not cellular over time. The generally large values of δ/k in all the roughness experiments reported here ensure that (2) and (3) in §4.1 can be used to describe the rough-wall velocity profiles.

The ratios δ/k and w/k determine the curvature of waviness of the mean streamlines in the neighbourhood of the roughness elements. The present lowest δ/k is higher than those of Antonia & Luxton (1971) and Perry *et al.* (1969). Since w/k is approximately the same in these three k-type experiments, a higher δ/k should mean reduced streamline waviness. Such waviness complicates the analysis of a control volume taken around a roughness element owing to the presence of a shear-stress term from the mean flow, viz. UV (Antonia & Luxton 1971). Here U and

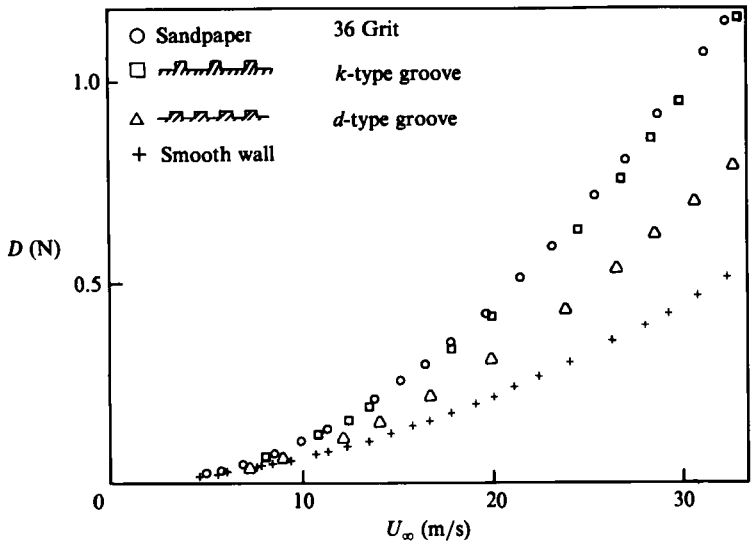

FIGURE 3. Drag characteristics of a 91.5 cm long × 28 cm wide surface.

V are the local mean velocities along the x- and y-directions respectively. The quantitative effect of UV is not yet known. But, since δ/k is large, the effect of the waviness of the streamlines is presumed to be small in the present experiments.

The results for two sandgrain sizes are considered. The grain sizes are nearly uniform. Grit 36 was chosen because its drag versus speed characteristic is virtually the same as that in the k-type groove (figure 3). This allows comparisons between the two surfaces. The sandgrains used are sandpapers 23 cm × 28 cm in size which are stuck to the surface using double-sided tapes. In one experiment, the entire 6.28 m length of the splitter plate is covered with cloth-backed grit 50 sandpapers (table 2). This may be one of the largest lengths of sandgrain-roughened wall studied in a laboratory so far and allowed verification of the existence of Rotta's condition of self-preservation. In the 7 in. × 11 in. tunnel (§2.2), the plates containing the groove and sandgrain roughnesses are aligned such that the tips of the roughness elements are at the same level as the upstream smooth wall. This prevents the formation of any separation bubble at the leading and trailing edges of the flat-plate model. This alignment is crucial in the drag-balance measurements.

2.2. *Wind tunnels*

The test-plate configurations are given in table 2. The experiments were performed in two low-speed wind tunnels. All boundary layer surveys on the k- and d-types of grooved roughness and all drag-balance and hot-wire measurements were made in the Langley 7 in. × 11 in. Low-Speed Wind Tunnel located in the Viscous Flow Branch. The boundary-layer surveys on the sandgrain roughness were made in the 2 ft. × 3 ft. Boundary Layer Channel also located in the Viscous Flow Branch.

The 7 in. × 11 in. tunnel is of the return-circuit closed-test-section type (Bandyopadhyay 1986). Following a suggestion by Mr D. M. Bushnell, the contraction was provided with a rather short concave region followed by a much more gradual convex length. This design minimized the contamination by Taylor–Görtler vortices in the test-section floor. This could be relevant since measurements were taken on the test-section floor rather than on a splitter plate. The maximum tunnel speed was

	Roughness	Tunnel	Test plate	Boundary-layer trip	Smooth wall length between trip and rough wall	Rough wall length	Origin of longitudinal distance, x	U_∞(m/s)
(*a*)	*d*-type groove	7 in. × 11 in.	Tunnel floor	1.5 mm diameter rod	26 cm	91.5 cm	At the start of rough wall	various
(*b*)	*k*-type groove	7 in. × 11 in.	Tunnel floor	1.5 mm diameter rod	26 cm	91.5 cm	At the start of rough wall	various
(*c*)	36 grit sandgrain	7 in. × 11 in.	Tunnel floor	1.5 mm diameter rod	26 cm	91.5 cm	At the start of rough wall	various
(*d*)	50 grit sandgrain	2 ft. × 3 ft.	Splitter plate	5 cm long 36 grit sandgrain on profiled leading edge	2.264 m	4.016 m	At the leading edge of splitter plate	40
(*e*)	50 grit sandgrain	2 ft. × 3 ft.	Splitter plate	5 cm long 36 grit sandgrain on profiled leading edge	Nil	6.28 m	At the leading edge of splitter plate	40

TABLE 2. Test-plate configurations

about 40 m/s and the turbulence intensity in the test section was below 0.2%. The variation in temperature of the medium was less than 1 °F during a boundary-layer survey. The free-stream velocity was continuously monitored and the variation was less than 1% during a survey. The test section was 91.5 cm long and 18 cm × 28 cm in cross-section. One of the sidewalls was motorized to produce a taper in the test section to compensate for the boundary-layer growth and generate a zero pressure gradient in the streamwise direction. Spanwise measurement of momentum thickness θ at a smooth wall showed the effective region of the two-dimensional flow to reduce only slightly – from 20 cm at $x = -2.5$ cm to 18 cm at $x = 80$ cm owing to the corner flows. The reduction was higher – from 18 cm at $x = 35$ cm to 10 cm at $x = 80$ cm in the worst case, viz. the k-type grooved wall.

The 2 ft. × 3 ft. tunnel is also of the return-circuit closed-test-section type. The test section is 6.28 m long and 61 cm × 91 cm in cross-section. The boundary-layer surveys were performed on a 3 cm thick aluminium honeycomb sandwich splitter plate having a profiled leading edge and mounted horizontally in the test section. The roof above this plate was slightly tapered to generate a zero pressure gradient. The surveys were made at a free-stream speed of 40 m/s which could be held within 0.5% during a run. The free-stream turbulence intensity was 0.1% in the test section. Both the tunnels were equipped with computer-controlled probe traverse mechanisms. The probe movement was measured by optical encoders to within ± 0.05 mm.

2.3. *Measurement procedure*

One of the troublesome areas of rough-wall investigations is the determination of the local wall resistance. The procedure followed is discussed in §4. To provide an independent, although indirect, check on these estimates, the drag experienced by an area of about 28 cm wide × 91.5 cm long of the test-section floor occupied by the roughness model was measured by a drag balance (designed by Dr L. M. Weinstein) in the 7 in. × 11 in. tunnel (Bandyopadhyay 1986). The model was made free floating by supporting it on an air bearing. The drag was measured by the deflection caused on a beam which was measured by a pair of piezoresistive strain sensors. The drag range of operation was 0.03 to 2 N. Typically, a drag of 1 N caused a horizontal deflection of 0.1 mm. The balance was calibrated against known weights. The calibration slope remained virtually the same over the full range and showed no drift over a period of six months. To keep the model free floating, it was provided with a gap of about 1 mm at the leading and trailing edges and at the junctions with the sidewalls. Any leakage through these gaps was virtually eliminated in two ways. First, the test-section pressure gradient was set to zero at each free-stream speed by moving one sidewall. Secondly, a large jacket was built around the test section and a continuous suction was provided to balance the static pressures between the test section and the jacket. Typically, a variation of ± 0.5 Pa in the jacket/test-section differential pressure was found to cause a change of only ± 0.7% in the drag. In most of the speed ranges it was possible to set the differential pressure to within a much smaller range. The uncertainty in the drag measurements was established by repeating the measurements after turning the model by 180° and realigning it afresh. The drag measurements could be reproduced to within ± 1.5%.

The mean-velocity profiles were measured using flattened Pitot tubes and electronic manometers. The measurements of momentum thickness θ could be reproduced to within ± 0.6%. The hot-wire measurements were taken using a straight prong, 1 mm long, platinum-coated tungsten single wire 5 μm in diameter and a constant-temperature anemometer whose output was linearized. The digitization of the output

signal and the computations of short-time autocorrelation were done using a programmable processor. The shortest sampling time was 10 μs.

3. Self-preservation

The streamwise distributions of the boundary-layer integral quantities viz. momentum (θ), displacement (δ^*) and boundary-layer (δ) thickness and shape factor (H) are shown in figures 4 and 5 for the d- and k-type groove roughness respectively. In

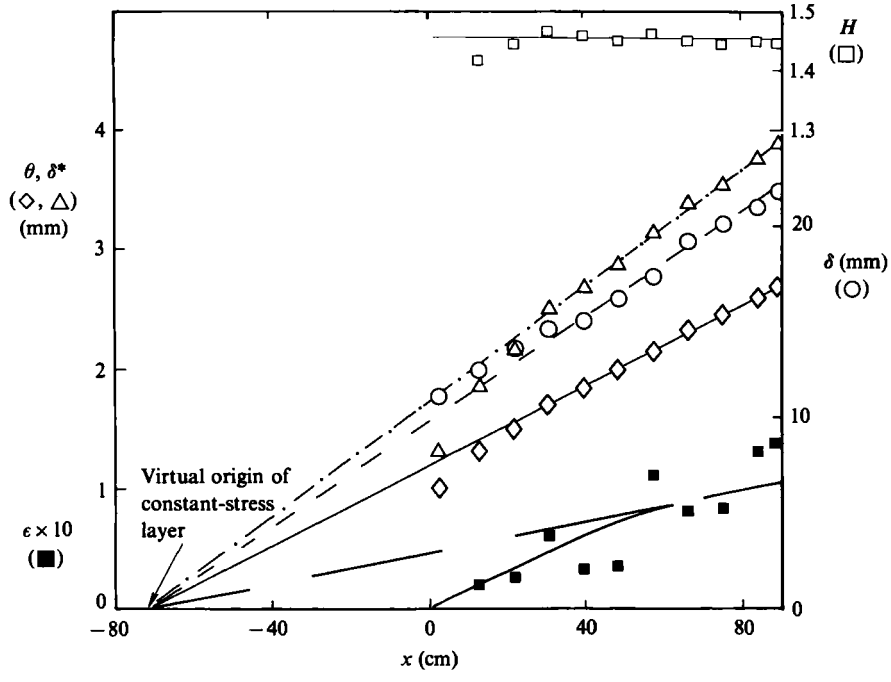

FIGURE 4. Distributions of integral quantities in a d-type grooved wall; $U_\infty = 27.5$ m/s.

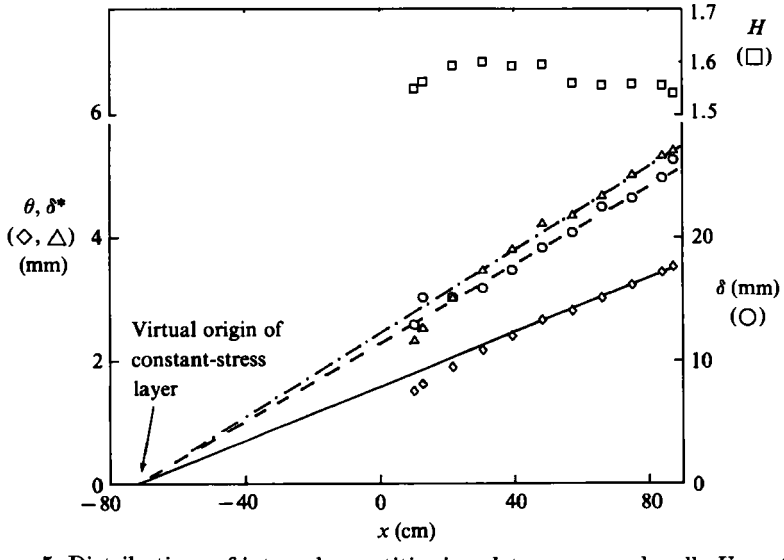

FIGURE 5. Distributions of integral quantities in a k-type grooved wall; $U_\infty = 28$ m/s.

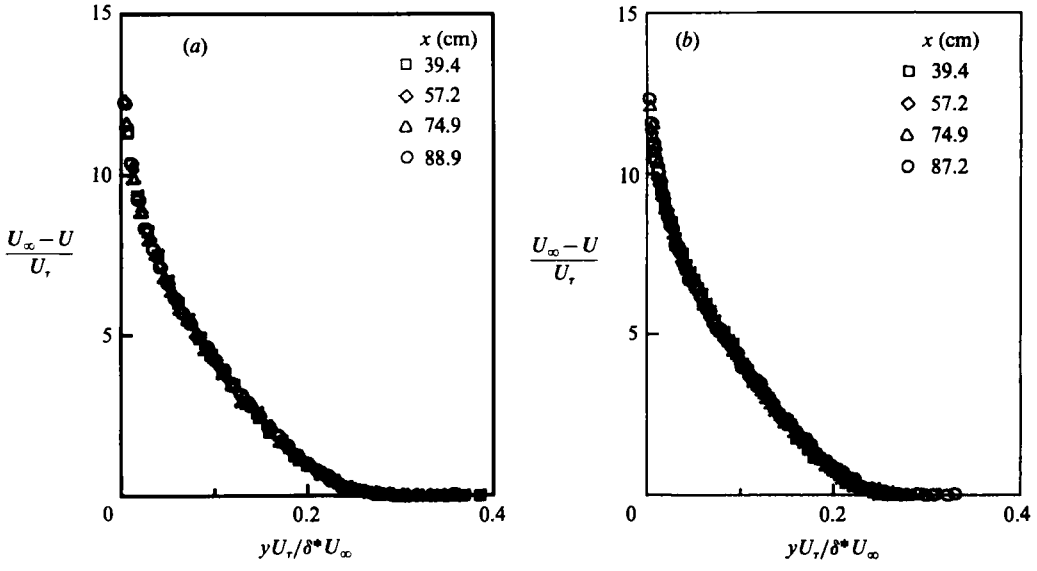

FIGURE 6. Defect-layer similarity in (*a*) *d*-type and (*b*) *k*-type grooved walls.

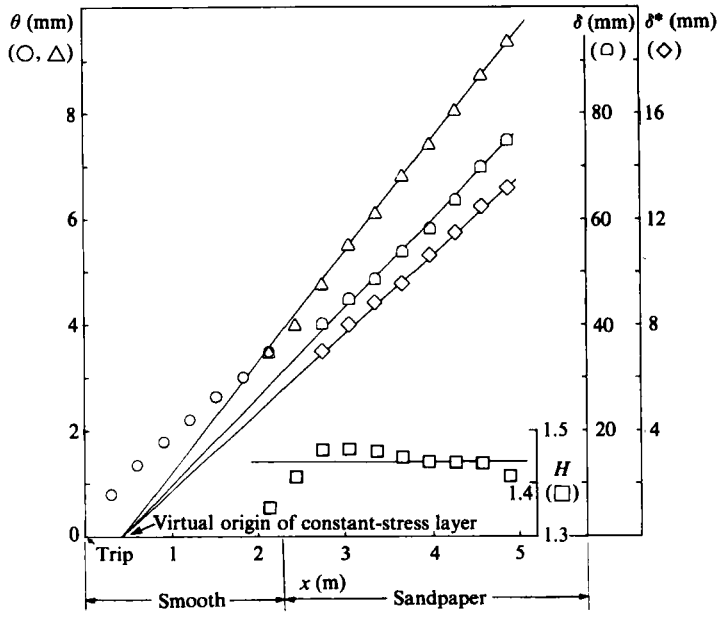

FIGURE 7. Distributions of integral quantities in a smooth-to-rough (sandgrain) wall; $U_\infty = 40$ m/s.

both, the roughness starts at $x = 0$ and is preceded by a smooth wall. In the *d*-type wall, the shape factor reaches a nearly constant value after $x = 20$ cm; but the *k*-type wall shows such a tendency only beyond 60 cm. In the similar *k*-type grooved-wall experiments of Antonia & Luxton (1971) H also reaches a nearly constant value after a similar distance. In the region of constant H, the integral quantities have a linear variation and have a common virtual origin. Figure 6(*a*, *b*) shows that the velocity-

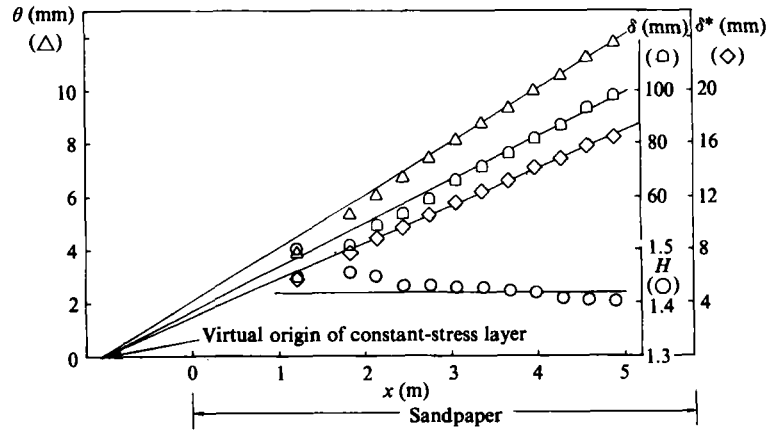

FIGURE 8. Distributions of integral quantities in a sandgrain-roughened wall; $U_\infty = 40$ m/s.

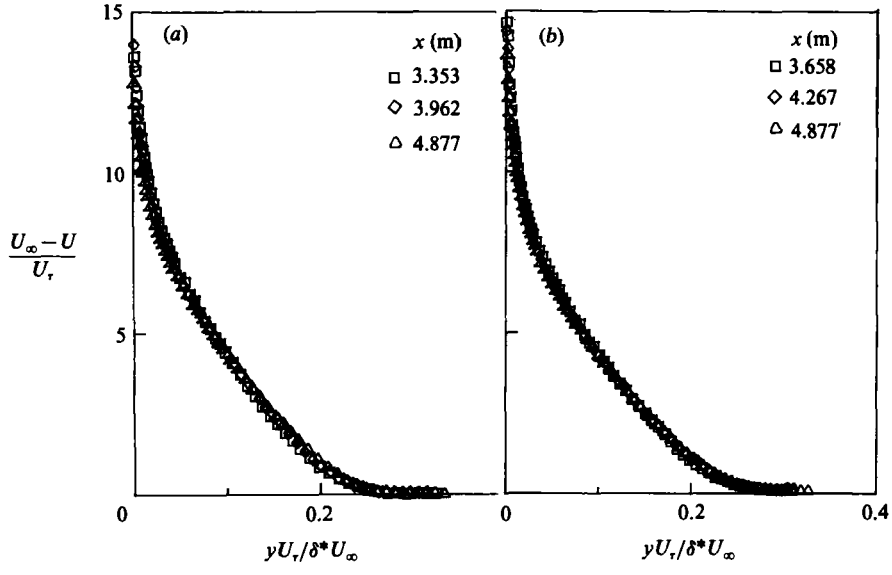

FIGURE 9. Defect-layer similarity in sandgrain-roughened walls; (*a*) smooth-to-rough case and (*b*) full-length rough case; $U_\infty = 40$ m/s.

defect profiles are self-similar in the region of constant H. The above kinematic results indicate that near-self-preservation has been reached earlier in the d-type grooved wall. The k-type grooved wall also probably reaches such a state, but the present wall length is too small to confirm that. Perry *et al.* (1969) have shown that Rotta's (1962) condition of self-preservation is satisfied by a d-type wall. The present results verify that finding. After the present work was completed, it was found that Osaka *et al.* (1982) had also verified the existence of self-preservation in a d-type wall.

The growths of the above boundary-layer integral quantities in sandgrain-roughened walls are shown in figures 7 and 8 for a smooth-to-rough and a full-length rough wall respectively. The wall shear stress reaches a constant level for both walls. In the region of constant wall shear stress, the thicknesses vary linearly and have

a common virtual origin; thus, H is also constant. Figure 9 shows the self-similar nature of the velocity-defect profiles in that region. Thus, the kinematic results in figures 7–9 indicate that Rotta's condition of self-preservation is reached by the mean flow in a (sandgrain-roughened) k-type wall also. A k-type distributed roughness requires an order-of-magnitude-longer length than a d-type wall to reach such a state. This result has not been reported earlier probably because most sandgrain rough-wall experiments have not been done on a long enough test plate. It will be interesting to see if the rough-wall boundary-layer structure scales in the self-preserving region have also reached a state of kinematic equilibrium.

4. Local wall shear stress

The problems associated with the determination of the local wall resistance in a rough wall boundary layer are well known. The heights of the two-dimensional grooved roughnesses studied here are rather small and it is not practical to determine the pressure component of the drag by pressure tapping the individual roughness elements. Also, in the transition regime of roughness, the pressure component does not constitute the total drag because the viscous frictional part is non-zero. In the following, the method used to determine the local wall shear stress and checks made thereto, are described.

4.1. *Determination of wall resistance from mean-velocity profiles*

An origin (figure 20) is required to represent the rough-wall mean-velocity profiles in the conventional boundary-layer format. However, the determination of this origin presupposes a knowledge of the local wall shear stress. In the present work,

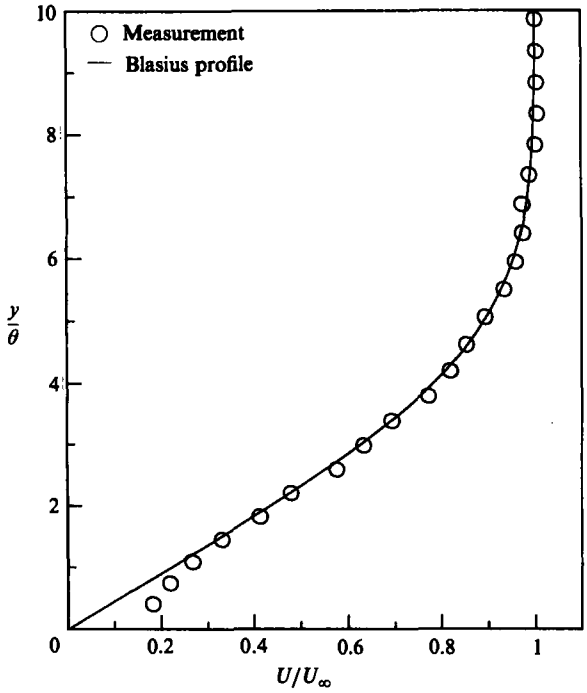

FIGURE 10. Laminar velocity distribution over a k-type grooved rough wall compared with Blasius profile; $Re_\theta = 270$.

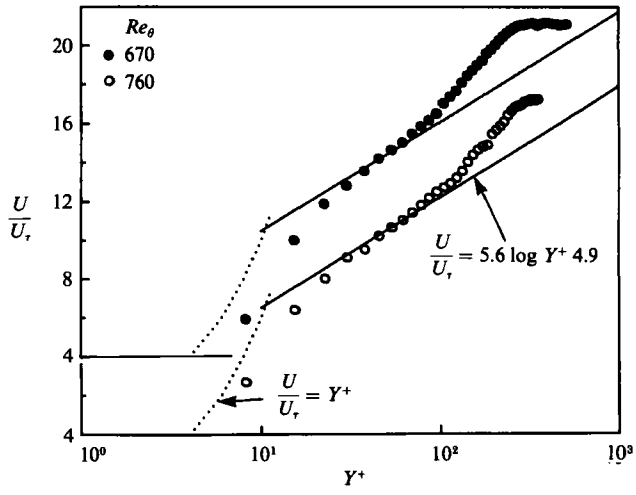

FIGURE 11. Low-Reynolds-number mean-velocity distributions over a k-type grooved rough wall compared with the law of the wall over a smooth surface.

this involved a minor iterative process. The procedure followed in the determination of the origin in y is described in §5.1.

Since roughness does not have any effect on the mean flow in the regime of hydraulic smoothness, it was thought that analysing the velocity profiles at low Reynolds numbers would be instructive. This exercise also provided an independent confirmation of the fact that in the downstream region of the k-type wall, the y-origin is located virtually at the bottom of the groove. Figure 10 shows a laminar velocity profile over the k-type groove wall measured at a free-stream speed of 2.5 m/s at $x = 66$ cm. The y-origin in this figure (and in figure 11) has been assumed to be at the bottom of the groove because the station is far downstream from the region of initial smooth-to-rough changeover. The measured profile agrees well with the Blasius profile (except in a small region near the wall), the θ-values being within 4% of each other. The roughness Reynolds number $U_\tau k/\nu$ of the layer is 1.6. The virtual-distance Reynolds number of the profile ($U_\infty x'/\nu$) is 1.66×10^5, which is less than the critical Reynolds number of 5×10^5 to 10^6 on a smooth flat plate.

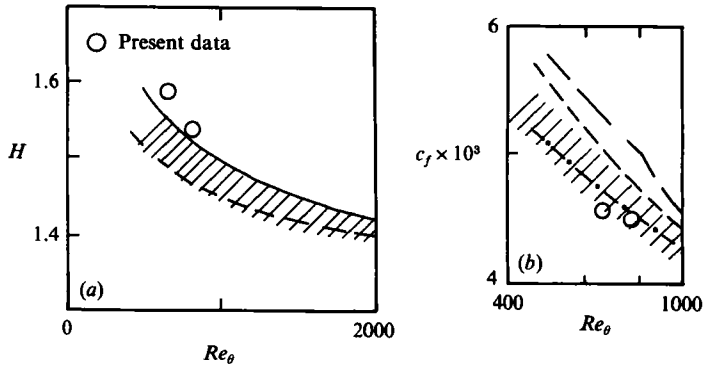

FIGURE 12. (a) Low-Reynolds-number rough-wall shape factor and (b) coefficient of skin friction compared with results in a smooth flat plate (from Purtell *et al.* 1981; ——, Landweber; – – –, Coles; –·–, Schoenherr; ——, Granville; smooth-wall measurements fall in the hatched region).

There is no information available on the nature of the laminar-to-turbulent transition over a grooved wall (Güven, Farel & Patel 1983). The mean-velocity profiles have been measured in the fully turbulent flow over the k-type grooved wall at $x = 66$ cm at an $U_\tau k/\nu$ of about 4. Two profiles are shown in figure 11. The momentum-thickness Reynolds numbers $Re_\theta(U_\infty \theta/\nu)$ are 670 and 760. The y-origin is taken at the bottom of the groove. The smooth-surface law of the wall has been fitted as shown to determine the coefficient of local skin friction c_f. Figure 11 shows a slight increase with Re_θ in the extent of the log layer in wall coordinates as has been observed by Purtell, Klebanoff & Buckley (1981) in a smooth flat plate. The c_f, H and Re_θ values are then compared in figure 12 with the recent low-Reynolds-number measurements and compilation of data by Purtell *et al.* The agreement between the rough- and smooth-wall data is reasonable. These results show that the rough wall being examined is well behaved.

The local wall shear stress was determined from the mean-velocity profiles in the following way. Measurements in rough-wall boundary layers usually do not penetrate the viscous sublayer and rarely cover most of the buffer layer. Clauser (Hama 1954) has described the velocity profile in the logarithmic part as

$$\frac{U_\infty - U}{U_\tau} = -\left(5.6 \log \frac{yU_\tau}{\delta^* U_\infty} + 0.6\right), \tag{2}$$

applicable in the inner region $yU_\tau/\nu \geqslant 32.5$ and $yU_\tau/\delta^* U_\infty \leqslant 0.045$ and Hama (1954) described the profile in the outer layer by the empirical relationship

$$\frac{U_\infty - U}{U_\tau} = 9.6\left[1 - \frac{y}{0.30\delta^* U_\infty/U_\tau}\right]^2, \tag{3}$$

which applies in the region $0.15 \leqslant y/\delta \leqslant 1$ for zero pressure gradient and low-free stream-turbulence-level flows (Monin & Yaglam 1971).

Equation (3) is another description of the so-called 'law of the wake'. Equations (2) and (3) connect smoothly at $y/\delta = 0.15$ or $yU_\tau/\delta^* U_\infty = 0.045$. Furthermore these two equations describe the velocity profiles no matter whether the wall is smooth or rough. With the availability of convenient graphics software packages it is a relatively easy matter to choose a value of U_τ by trial such that (2) and (3) will describe the measured profiles. The steps followed to determine the final values of U_τ and ϵ are given below. In the 7 in. × 11 in. tunnel, the variation in the smooth-wall c_f with x appeared to be small for first-estimate purposes; for a start, the variation was assumed to be small in the rough walls as well ignoring the jump in c_f at the upstream end. This allowed the plate-drag measurements (§4.2) to be used to determine the first estimates of U_τ. In the 2 ft. × 3 ft. tunnel, the $\mathrm{d}\theta/\mathrm{d}x$ values were used to obtain the first estimates. On the other hand, first estimates of ϵ were obtained by studying the trend in the literature: in a k-type groove, somewhat away from the smooth-to-rough transition, ϵ was taken to be equal to k; in a d-type groove, ϵ was zero at $x = 0$ and was assumed to increase linearly (in view of self-preservation) to $\frac{1}{2}k$ at $x = 90$ cm. Thus the first estimate of the y-origin was assumed to be near the groove top in the d-type and near the groove bottom in the k-type grooved walls. Holding ϵ at the first estimate, the best velocity-profile match was then searched by trial and error to determine what turned out to be the final U_τ in most cases. The final value of ϵ was then obtained by the method of Furuya *et al.* (1976) (§5.1) using the just-calculated U_τ. This final ϵ, however, was not found to affect the U_τ used in its estimation except in the far-upstream regions of the rough walls. The roughness

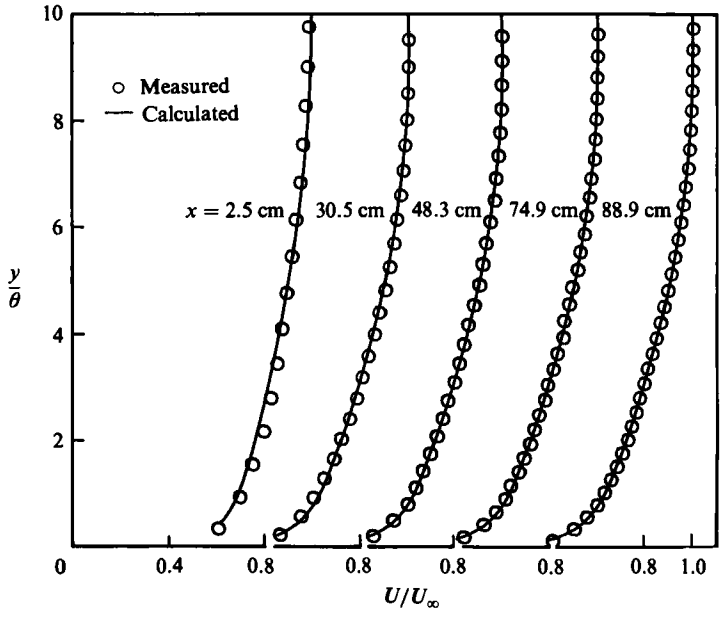

FIGURE 13. Typical set of measured and calculated velocity profiles in the d-type wall: $U_\infty = 27.5$ m/s.

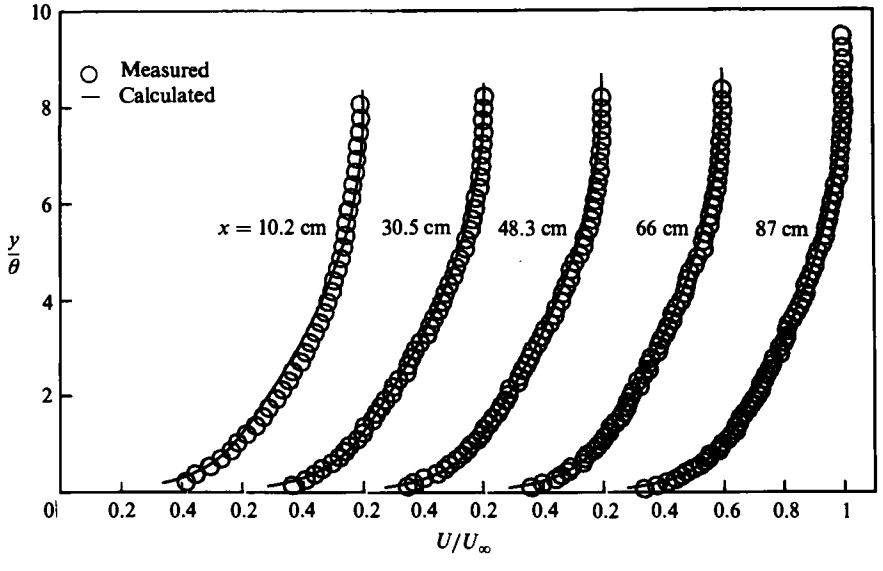

FIGURE 14. Typical set of measured and calculated velocity profiles in the k-type grooved wall: $U_\infty = 28$ m/s.

function was calculated using the final estimates of U_τ. Since this method has not been used previously it requires a closer scrutiny.

The popular Clauser chart method of determining local wall shear stress in a smooth wall also is basically a profile matching technique. However, since it does so only in the logarithmic region, which is thin, frequently there are only a few data points to work with. In contrast, the present profile matching covers virtually the entire profile.

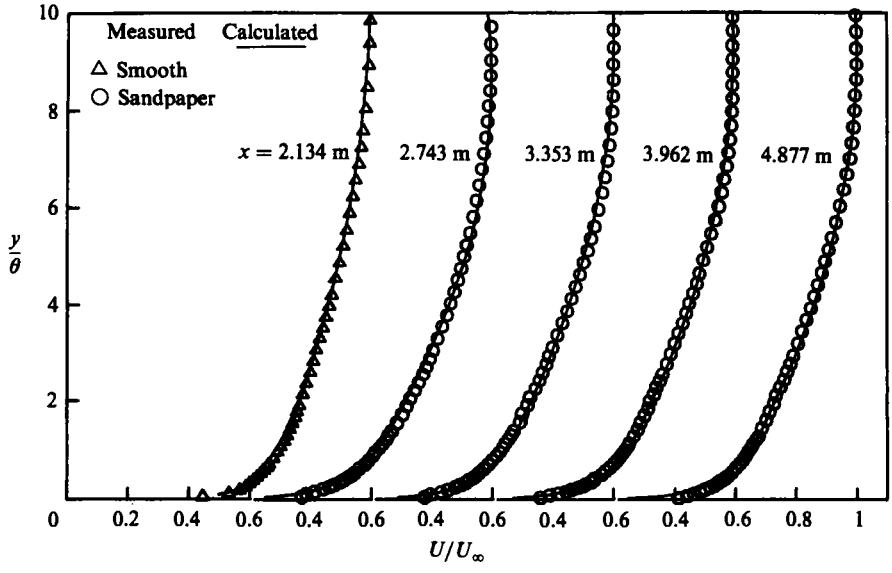

FIGURE 15. Typical set of measured and calculated velocity profiles in the smooth-to-rough (sandgrain) wall.

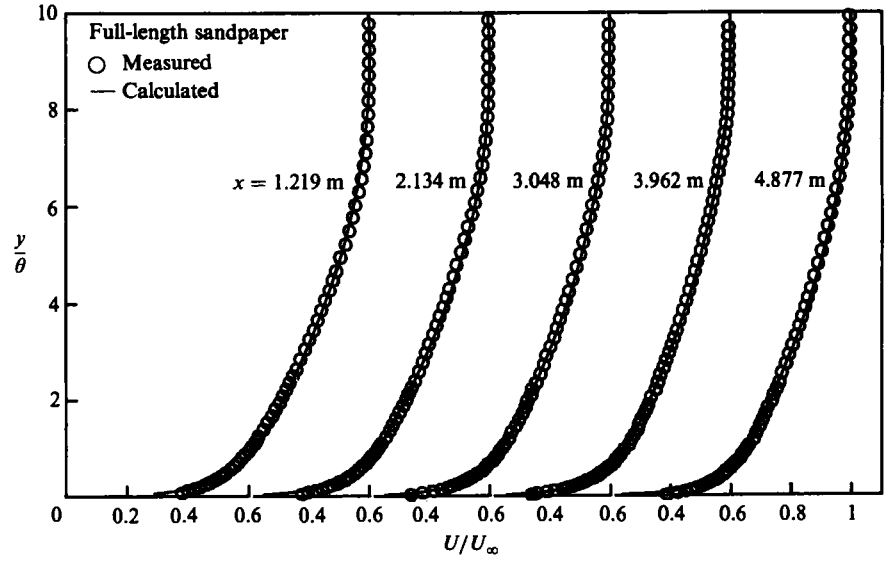

FIGURE 16. Typical set of measured and calculated velocity profiles in the full-length sandgrain-roughened wall.

Figures 13–16 provide examples showing the quality of match between the measured and calculated profiles in the wall configurations (*a*), (*b*), (*d*), and (*e*) in table 2. The U_τ involved in these calculated profiles have been used as the final estimate. The measured and calculated profiles have also been plotted in a defect-law form, to examine the near-wall region closely. Except in a small upstream region in the *k*-type grooved wall, where there is an abrupt change in the boundary condition, all measured and calculated profiles agree well.

Two preliminary checks were made on the wall-shear-stress values obtained by the

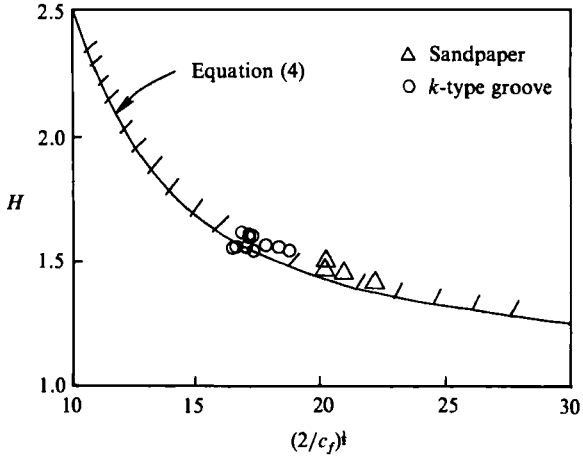

FIGURE 17. Skin-friction results obtained by profile matching compared with (4); the hatched area indicates where the smooth and rough wall data of Schultz-Grunow and Hama (1954) fall.

above procedure. The first was provided by the measurements made on a smooth wall as shown in figure 15. The wall shear stress in a smooth wall was measured by a Preston tube, Clauser chart and Ludwieg–Tillman relationship. The present method yielded c_f values in good agreement with these conventional smooth-wall methods. The second check was made in the self-preserving flows over a sandgrain roughness where the wall shear stress could be obtained accurately by employing the momentum integral equation. The two wall-shear-stress values were in reasonable agreement.

An indirect check on the method is provided in figure 17 where the present sandgrain and k-type grooved-rough-wall data are compared with those of Hama (1954). The agreement is very good. All the measurements also agree with the relationship

$$H = [1 - G(\tfrac{1}{2}c_f)^{\frac{1}{2}}]^{-1}, \tag{4}$$

where

$$G = \int_0^\infty \left[\frac{U_\infty - U}{U_\tau}\right]^2 d\left(\frac{yU_\tau}{\delta^* U_\infty}\right).$$

The value of G used is about 6.1 as found in a zero-pressure-gradient smooth-flat-plate boundary layer.

4.2. *Drag measurements*

Finally an independent, although indirect, check has been made on the above procedure of velocity-profile matching to determine the local wall shear stress. Drag-balance measurements have been performed on 91.5 cm long × 28 cm wide smooth and rough surfaces. The measurements are shown in figure 3. These drag measurements also provided the first estimate of the wall shear stress to be used in the procedure of profile matching by trial. The centreline streamwise variation in c_f is then obtained by the above method; figure 18 is an example of c_f obtained in the k-type grooved wall at a free-stream speed of 28 m/s; the uncertainty in the c_f values is about ± 0.0002. The figure also shows the c_f estimates obtained from the momentum integral equation. When these estimates are used in a plot like figure 17, the agreement with (4) and Hama's results turns out to be poor. Assuming a two-dimensional nature for the limiting streamlines, the drag on the 91.5 cm × 28 cm

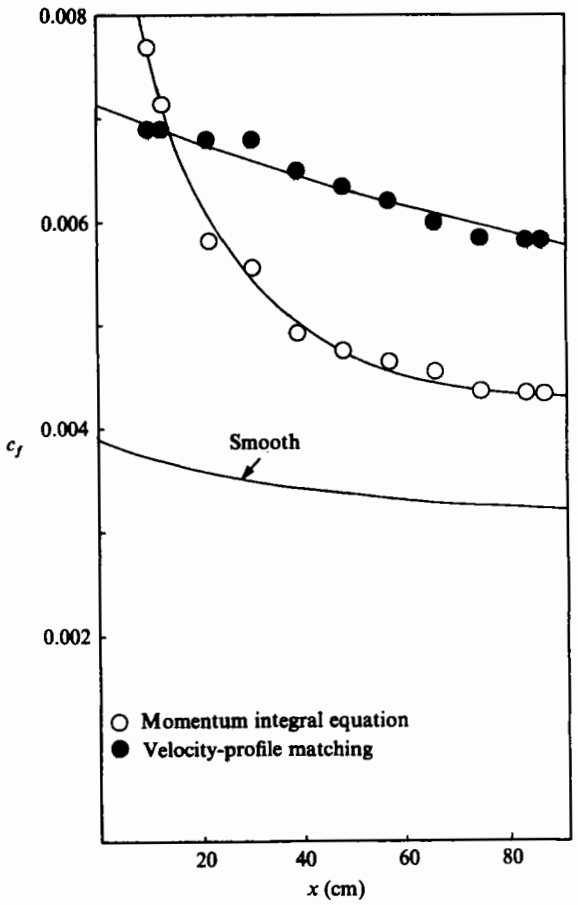

FIGURE 18. Distribution of c_f obtained by velocity-profile matching compared with that from the momentum integral equation: k-type groove roughness; $U_\infty = 28$ m/s.

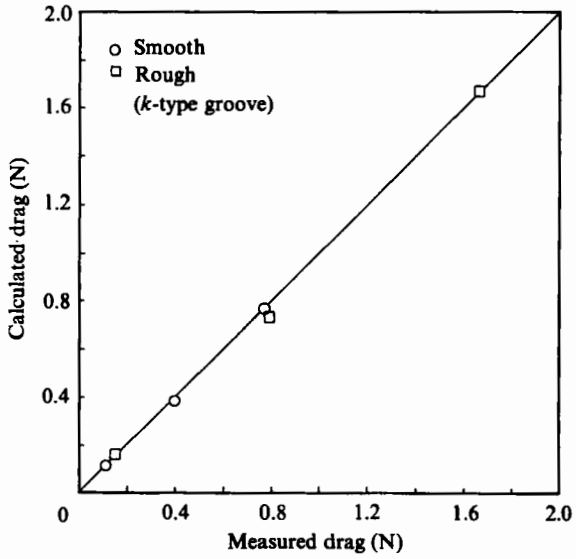

FIGURE 19. Drag-balance measurements on a 91.5 cm long × 28 cm wide surface compared with calculated values.

plate has been calculated using the c_f values obtained by both the momentum integral and profile matching methods. The momentum integral results do not agree well with the direct drag measurements. However, as figure 19 shows, the drag values based on the profile matching method agree well with the drag-balance measurements. Consequently, all local wall-shear-stress values reported in this paper have been obtained by the profile matching method.

5. Lengthscales in a smooth-to-groove wall

5.1. *Error in origin*

During measurements, the y-distances have been measured from the tips of the local roughness elements (figure 20). However, to arrive at a logarithmic velocity distribution, which is assumed to exist for a rough wall as well as for a smooth wall, the y-origin has to lie some distance below the tips of the roughness elements. This distance ϵ is called the error in origin. Perry *et al.* (1969) have suggested that it is a measure of the interaction between the mean flow and the roughness. They have also developed a modified Clauser plot to determine ϵ. Perry *et al.* could successfully use this method because, in their adverse-pressure-gradient experiments, ϵ is larger. However, in the present experiments, their method could not be used satisfactorily because the pressure gradient is zero and both k and ϵ are rather small. In comparison to Perry *et al.*, Furuya *et al.* (1976) have proposed a more straightforward method. This has been used in the present study and is briefly described below.

Let the displacement thickness in the y_T and y-coordinates (figure 20) be δ_T^* and δ^* respectively such that

$$y = y_T + \epsilon,$$

and

$$\delta^* = \delta_T^* + \delta_\epsilon^*,$$

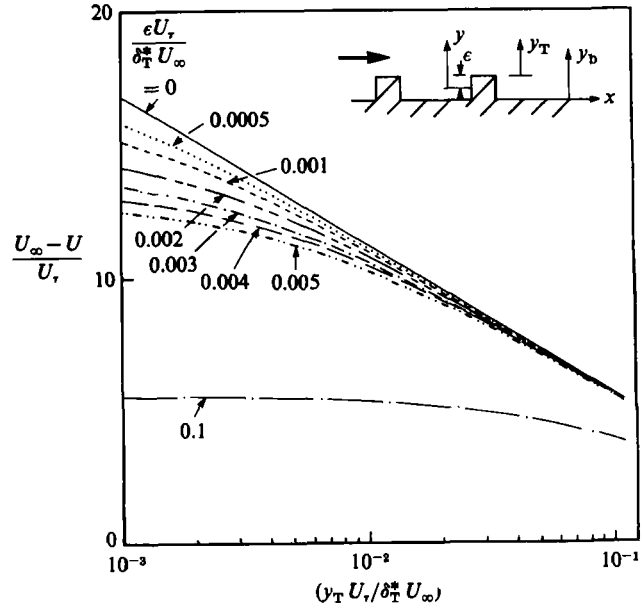

FIGURE 20. Plot used to determine the error in the origin by the method of Furuya *et al.* (1976).

where, δ_ϵ^* is the displacement thickness in the range $0 \leqslant y \leqslant \epsilon$. Substituting these in (2), the following relationship is obtained:

$$\frac{U_\infty - U}{U_\tau} = -5.6 \log \frac{y_T U_\tau}{\delta_T^* U_\infty} - 5.6 \log\left[1 + \left(\frac{\epsilon U_\tau}{\delta_T^* U_\infty}\right)\left(\frac{y_T U_\tau}{\delta_T^* U_\infty}\right)^{-1}\right] + \left[5.6 \log\left(1 + \frac{\delta_\epsilon^*}{\delta_T^*}\right) - 0.6\right]. \tag{5}$$

Equation (5) is plotted in figure 20 for various values of the parameter $(\epsilon U_\tau)/(\delta_T^* U_\infty)$. The last bracketed term in (5) is constant at a station and has been ignored in the plot because it merely displaces the plot bodily. The measured profiles are superposed on figure 20 and ϵ is determined from the parameter that allows agreement with the measurements.

Two mean-flow lengthscales describe the region of changeover from smooth to rough in a boundary layer developing over the grooved walls. They are the error in origin and the thickness of the internal layer. The growth of the error in origin in such step changes in roughness are shown in the lower plots in figures 4 and 21 in the *d*- and *k*-type grooved walls respectively. The location of the origin moves downwards from the tip of the roughness strip towards the bottom of the groove. An asymptotic value of ϵ, about equal to k, is reached at a distance of about $1000k$ in the *k*-type wall. In the constant-wall-shear-stress region, the ϵ-distribution in the *d*-type wall is expected to be linear as shown with a common virtual origin, but the scatter in the data is too large to confirm such a supposition.

5.2. *Internal layer*

When a smooth-flat-plate turbulent boundary layer encounters a rough surface, a rough-wall boundary layer starts developing within it. This is called the internal layer and has been studied in some detail in a *k*-type grooved wall by Antonia & Luxton (1971). By a dimensional argument they have shown that, in the region of a step

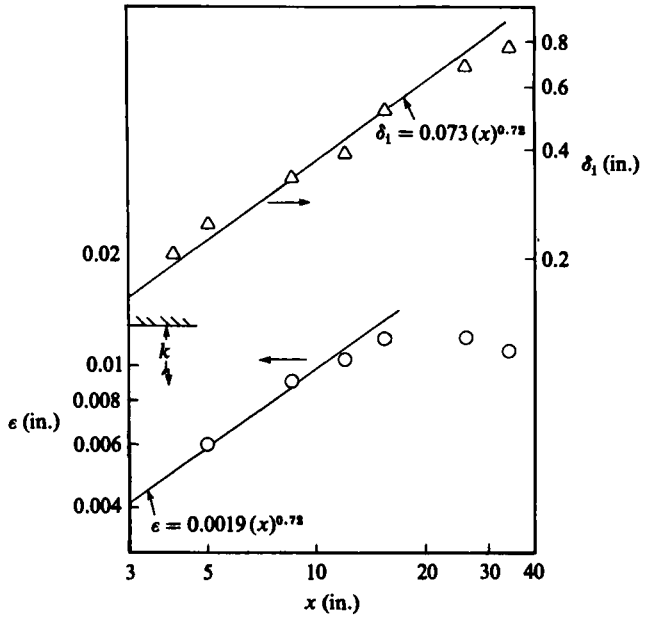

FIGURE 21. Error in origin compared with the internal-layer thickness in the *k*-type grooved wall; $U_\infty = 28$ m/s.

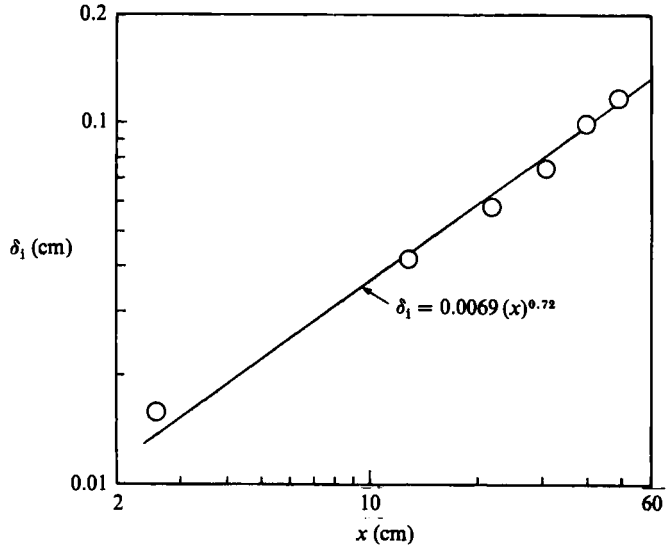

FIGURE 22. Internal-layer thickness in the d-type grooved wall; $U_\infty = 27.5$ m/s.

change in roughness, the flow can be described to a first order as adjusting from the smooth-wall level of the shear stress gradient $(\partial\tau/\partial y)$ to that in the rough wall. This behaviour leads to the relationship $U \sim y^{\frac{1}{2}}$. The velocity profiles over the upstream smooth wall and the k-type grooved wall have been plotted in U/U_∞ versus $y^{\frac{1}{2}}$ coordinates to determine δ_i, the thickness of the internal layer. This thickness has been taken as the 'knee' point; that is, the point at which the rough- and smooth-wall half-power straight lines meet. The distributions of δ_i are shown in figures 21 and 22 for the k- and d-type grooved walls respectively. The variation in the k-type wall is described by $\delta_i \sim x^{0.72}$, as has also been found by Antonia & Luxton (1971). Figure 22 shows that the 0.72-power growth rate of the internal layer holds in the d-type wall also and hence is independent of the type of roughness. Figure 21 shows that a 0.72-power line also describes the growth of the error in origin in the k-type wall. The similar growth rate of the internal layer and the error in origin suggests that ϵ is indicative of the rate of adjustment of the wall shear stress following the step change in roughness. In consistence with Rotta's (1962) condition, the rate of self-preservation has not been reached in the k-type grooved wall in the region of nonlinear growth of ϵ as shown in figure 21.

6. Roughness function

The roughness function was calculated from the following semilogarithmic relationship:

$$\frac{U}{U_\tau} = 5.6 \log \frac{yU_\tau}{\nu} + 4.9 - \frac{\Delta U}{U_\tau}. \tag{6}$$

The values of the multiplicative and additive constants recommended by the 1969 Stanford conference on the computation of turbulent flows are 5.62 and 5.0 respectively. However, the values in (6) have been used to conform with the notable rough-wall works of Clauser and Hama. The present roughness-function results obtained in the sandgrain and k-type grooved wall are compared with other authors' results in figure 1. The limited sandgrain results from the present experiments agree

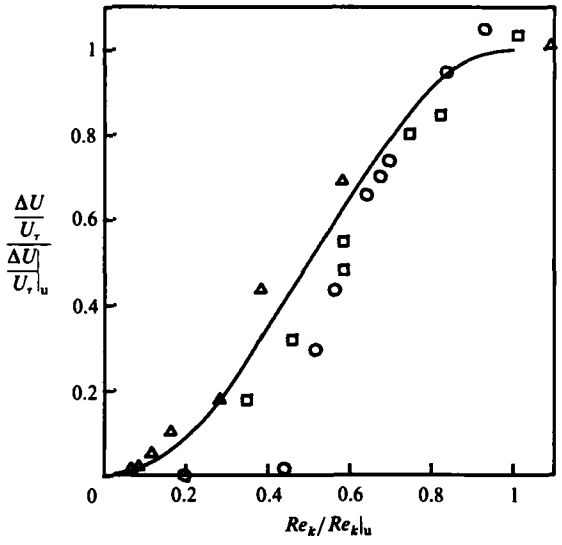

FIGURE 23. Roughness-function similarity in the transition regime; △, sandgrain–Colebrook & White (1937); □, wire mesh – Hama (1954); ○, k-type two-dimensional groove – present data; ——, equation (7).

very well with those of Colebrook & White (1937). In the fully rough regime, the present k-type-groove results fall on the same line as Moore (1951) and Perry & Joubert (see Perry *et al.* 1969). The groove dimension w/k is about the same in all these experiments. However, the most significant result is that the upper limit of the transition regime $(U_\tau k/\nu)_u$ in the two-dimensional roughness has indeed the lowest value. This provides strong support for the initial hypothesis that $(U_\tau k/\nu)_u$ drops with increasing aspect ratio of the roughness elements. Further evidence is presented in the following.

If the above hypothesis is correct, it implies that the apparently characteristic behaviours of the roughness function in the transition regime are actually similar except that they are scaled as appropriate to the particular aspect ratio of the roughness element. The distributions of the roughness function in the transition regime from the three roughnesses shown in figure 1 have been normalized by the appropriate $(kU_\tau/\nu)_u$ and the value of $\Delta U/U_\tau$ at that Reynolds number. The result is shown in figure 23 which also includes a modified cosine curve fit, viz.

$$\frac{\Delta U/U_\tau}{(\Delta U/U_\tau)_u} = 0.5\left[1-\cos\left\{\pi\frac{(U_\tau k/\nu)}{(U_\tau k/\nu)_u}\right\}\right]. \tag{7}$$

The collapse of the data is reasonable. With the above normalization, the roughness function is seen to have a universal behaviour in the transition regime irrespective of the type of roughness.

In addition, consider the following. In the fully rough regime, the roughness function versus the roughness-Reynolds-number relationship (figure 1) is given by

$$\frac{\Delta U}{U_\tau} = 5.6\log_{10}\left(\frac{kU_\tau}{\nu}\right)+C, \tag{8}$$

where C is a constant whose value depends on the type of roughness. As marked in

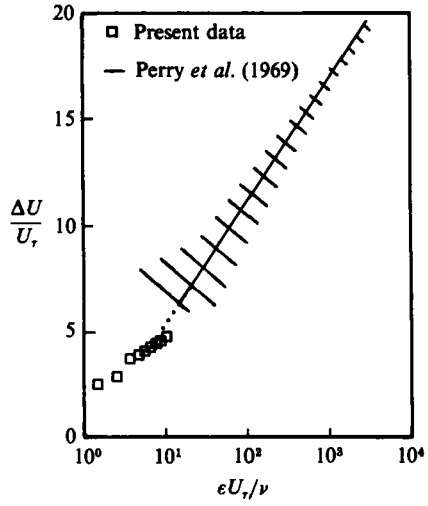

FIGURE 24. Roughness function in the d-type grooved wall; the cross-hatchings indicate the data band of Perry *et al.* (1969) and the straight line through the hatchings represents equation (9).

the fully rough regime in figure 1, C varies between the three roughnesses by F_1 and F_2. Further marks on that figure also show that once the upper limit of the transition regime $(kU_\tau/\nu)_u$ is known in any one roughness, the values of this limit in the remaining two roughnesses can be simply obtained from F_1 and F_2. Equation (8) indicates that only the slope of the semilogarithmic behaviour is universal. On the other hand, the present results indicate that the behaviour of the roughness function becomes self-similar in both the transition and fully rough regimes when the scaling factor $(kU_\tau/\nu)_u$ is taken into account. Thus, the upper limit of the transition-regime Reynolds number has an important place in the drag behaviour of k-type rough-wall boundary layers.

In a d-type wall nothing is known about the transition regime. In the fully rough regime, Perry *et al.* (1969) have shown that roughness function correlates with $\epsilon U_\tau/\nu$ rather than with kU_τ/ν as in a k-type wall. Figure 24 shows the present data plotted against $\epsilon U_\tau/\nu$. The solid line shows Perry *et al.*'s relationship, viz.

$$\frac{\Delta U}{U_\tau} = 5.76 \log_{10}\left(\frac{\epsilon U_\tau}{\nu}\right) - 0.4, \tag{9}$$

in the range of their data indicated by the cross-hatchings. Note that Perry *et al.* estimated ϵ by a different method and (9) represents a universal data correlation in both zero and adverse pressure gradients. The limited amount of present data indicate that (9) applies down to an $\epsilon U_\tau/\nu$ value of about 5 and there may be a transitional rough regime below that value.

7. A model of the transition regime in k-type roughness

It is well accepted that the lower critical transition Reynolds number indicates the onset of vortex shedding by the roughness elements. But what is the physical significance of the upper critical transition Reynolds number? Figure 1 shows that $(kU_\tau/\nu)_u$ decreases with increasing aspect ratio of the roughness elements. However,

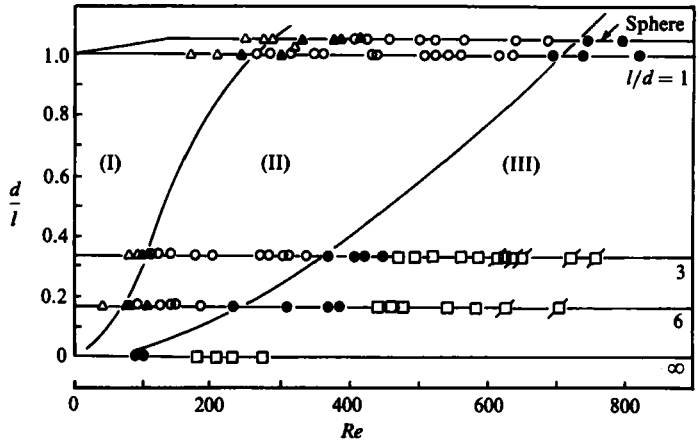

FIGURE 25. Figure 27 of Furuya & Miyata (1972); variation of the upper and lower critical Reynolds numbers of a wake with aspect ratio. Configuration in region I: stable thread-like; region II: regular vortex loops; region III: irregular vortex loops. Filled symbols show the transitional region; ⊓ shows the oscillation of necklace vortex.

this still remains a qualitative result. A quantitative verification of this could be obtained by making use of the stability diagrams obtained experimentally by Furuya & Miyata (1972). This is presented in the following.

Furuya & Miyata (1972) have visually observed the stability of the wakes of isolated roughness elements submerged in laminar boundary layers. The roughness elements studied were spheres and cylinders of aspect ratios (l/d) of 1 to ∞, their axes lying aligned along the span. Here l is the span and d is the diameter of the roughness element. The Reynolds numbers $Re(U_k d/\nu)$ at which the obstacles started shedding 'regularly arranged' horseshoe vortices and those at which the shedding became 'irregular' were noted. (Here U_k is the velocity at the roughness tip location in the absence of the roughness element.) In the smoke pictures of Furuya & Miyata, the wake looks markedly chaotic/turbulent when the authors deemed the shedding irregular whereas it is laminar-like when the shedding is regular. Furthermore, the individual horseshoe vortices develop 'wrinkles' when the shedding becomes irregular. It is likely that the wrinkling indicates the growth of higher harmonics and instability within the horseshoe vortex. The definition of the nature of the irregularity is admittedly imprecise at this stage and this aspect needs further investigation. But the appearance of the irregularity is unmistakable. The observations of Furuya & Miyata have been reproduced in figure 25. Their vortex loops are much like the horseshoe vortices found in low-Reynolds-number smooth-wall turbulent boundary layers (Head & Bandyopadhyay 1981). The necklace vortices, on the other hand, are more stable and their existence or the nature of their interaction with the horseshoe vortices in a rough-wall boundary layer is not known. In figure 25, between the roughnesses, note that the disparity between the values of the lower critical Reynolds number is much less than that of the upper critical Reynolds number. This behaviour is in accordance with the fact that the lower limit of the rough-wall transition regime varies only slightly for all 'uniform' roughnesses, but the upper limit varies considerably. The data on a sphere and cylinder of $l/d = 1$ in figure 25 indicate that, when the aspect ratio is approximately the same, the contouring of the surface of the roughness elements has only a marginal effect on the critical Reynolds numbers

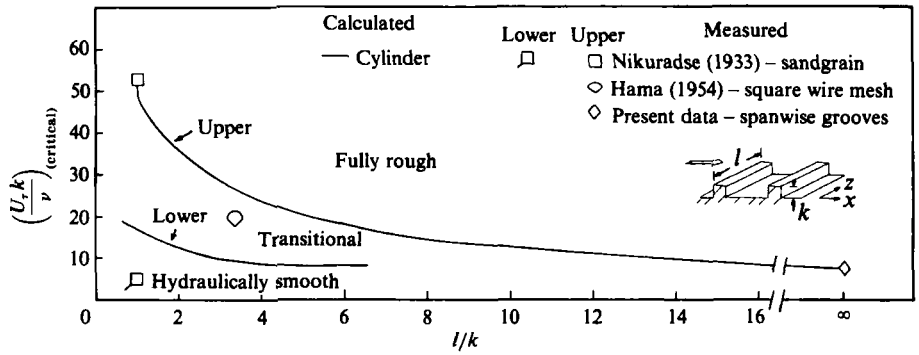

FIGURE 26. Relationship between upper and lower critical Reynolds numbers and aspect ratio of roughness elements in a rough-wall turbulent boundary layer.

although the effect on the Strouhal number is known to be markedly high. Making use of the regular law of the wall, the two stability lines in figure 25 have then been cast into those shown in figure 26.

The upper and lower solid lines in figure 26 indicate the variation of the upper and lower critical transition Reynolds numbers respectively with spanwise aspect ratio. The upper line has been compared with three data points from figure 1, viz. sandgrain, wire-mesh and two-dimensional grooves. The sandgrain is assumed to have an aspect ratio of one. More data is required to establish the behaviour for aspect ratios of less than one. In Hama's (1954) wire mesh, the aspect ratio changes over one pitch length and 3.6 has been taken as the mean value. Figure 26 shows that, for low aspect ratios, the lower critical line slightly overpredicts. The agreement between the measurements and the upper critical line is good. Therefore, we conclude that, in addition to the dependence of $(kU_\tau/\nu)_u$ on l/k, the figure also shows that the values of $(kU_\tau/\nu)_u$ in figure 1 correlate with the critical Reynolds numbers observed in the wakes of isolated roughness elements lying submerged in laminar boundary layers. A practical implication of the results is that, if the presence of roughness is unavoidable and a lower drag is desired, figures 1 and 26 show that a higher $(kU_\tau/\nu)_u$ should be aimed for. This can be achieved by making the roughness elements 'more three-dimensional'. The benefit will be noticeable below an aspect ratio of 6 to 8.

After the present work was completed, Dr P. S. Klebanoff drew the author's attention to the work of Smith & Clutter (1959) who examined the laminar-to-turbulent transition behind isolated roughness elements lying submerged in an otherwise laminar boundary layer. In their compilation of various authors' data, the 'three-dimensional roughness has shown greater values of $R_{k\,\text{crit}}$ than those for the two-dimensional roughness' (p. 236). Here, $R_{k\,\text{crit}}$ is defined as $U_k k/\nu$. The equivalent of $R_{k\,\text{crit}}$ in the present study is the lower critical roughness Reynolds number $(U_\tau k/\nu)_\ell$ which is indicated by the lower curve in figure 26. The trend in the present results and those of Smith & Clutter are in excellent agreement. (The reader should be cautioned that the results described in the Conclusions section of Smith & Clutter's paper (p. 243) contain a typographical error which gives a wrong sense of the trend.)

Further research is required to determine the physical significance of the upper critical Reynolds number in both an isolated roughness element and in a regular rough wall. In the case of an isolated roughness element in a laminar boundary layer, it is known that after the lower critical Reynolds number has been reached, increasing free-stream speed moves the point of transition closer to the roughness element

(Smith & Clutter 1959). Therefore, it seems likely that the previously mentioned onset of irregularity in the vortex-shedding experiments of Furuya & Miyata (1972) is a result of an interaction with the randomness accompanying transition. If this speculation is correct then $(U_\tau k/\nu)_u$ indicates the Reynolds number at which 'transition' takes place almost right behind the roughness elements. The extent of the roughness-function transition regime (figure 1) for any roughness can now be viewed as an indicator of the rate, which is characteristic of the roughness, at which transition moves upstream towards the roughness elements.

8. Vortex shedding in rough walls

In the previous sections it has been shown that the drag at a rough wall is closely related to the nature of the wake behind a similar roughness element lying submerged in an otherwise laminar boundary layer. This gives rise to the practically meaningful question: what is the relationship between drag and vortex shedding in a rough wall? This is addressed in the following.

In recent times, considerable effort has been devoted to unravelling the nature of the quasi-periodic turbulence-production cycle in smooth-flat-plate boundary layers. A similar cycle is in existence in a sandgrain-roughened wall also and the structure in most of the boundary layer is much the same as in a smooth wall (Grass 1971; Bessem & Stevens 1984). The transport of momentum and heat in rough walls would be decided by the quasi-cyclic nature of the wake of the roughness elements and therefore an investigation of the flow in the vicinity of the roughness elements would be useful. However, excepting the flow visualization work of Townes & Sabersky (1966) in two-dimensional square grooves, the flow in the neighbourhood of the roughness elements has not received much attention.

8.1. *Measurement of the time period of vortex shedding*

(i) *Velocity fluctuations.* To obtain an impression of the degree of periodicity present in the velocity fluctuations, the linearized signal from a single hot wire, located within the groove or behind a sandgrain, was examined while increasing the free-stream speed so that the state of the boundary layer changed gradually from laminar to fully rough. Figure 27 shows examples of the velocity fluctuations at low Reynolds numbers. The velocity traces shown in figure 27*a* (i to iv) are not taken simultaneously Figure 27 shows that the periodicity is clearer in the grooves than behind the sandgrain. Note also that the amplitude of the velocity fluctuations is smallest within the grooves. Figure 27*a* (i to iv) show that as the normal distance from the roughness elements is increased, the periodicity becomes progressively submerged in the background 'noise'. This indicates that the time period of vortex shedding can best be detected close behind the roughness elements.

(ii) *Short-time autocorrelation.* Although the velocity fluctuations on the oscilloscope were observed to be periodic, the rerise in the long-time autocorrelation tended to be rather weak. This implied that the vortex shedding was fairly periodic over short times and also that this time period varied randomly over a rather wide range over a long time. Thus, it was thought prudent to determine the mean time period of vortex shedding from many measurements of short-time autocorrelation. Figures 28–30 show examples of the distribution of short-time autocorrelation in the three rough walls at various speeds. At low speeds, only the *d*-type roughness was found to shed vortices in a rather low-noise background. About 3 to 5 vortices were shed

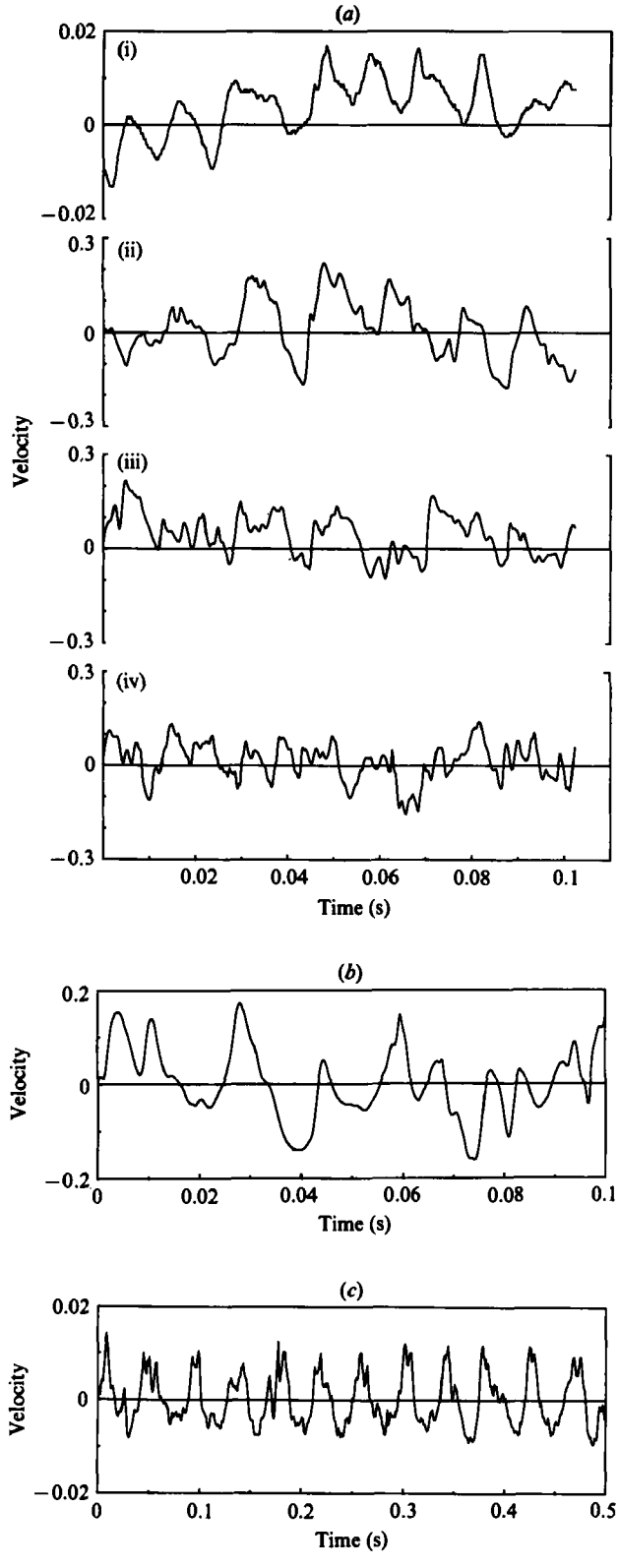

FIGURE 27. Quasi-periodicity in the velocity fluctuations in close proximity to the roughness elements at low roughness Reynolds numbers; $x = 66$ cm. (*a*) k-type grooved wall; $U_\infty = 3.66$ m/s; $x = 66$; $c/w = 0.4$: (i) $y_b/k = 0.77$; (ii) 5.2; (iii) 9.8; (iv) 18.2. (*b*) Sandgrain (grit 36); $U_\infty = 3.87$ m/s; $y_b/k = 1$. (*c*) d-type wall: $U_\infty = 5.58$ m/s; $c/w = 0.5$; $y_b/k = 1$.

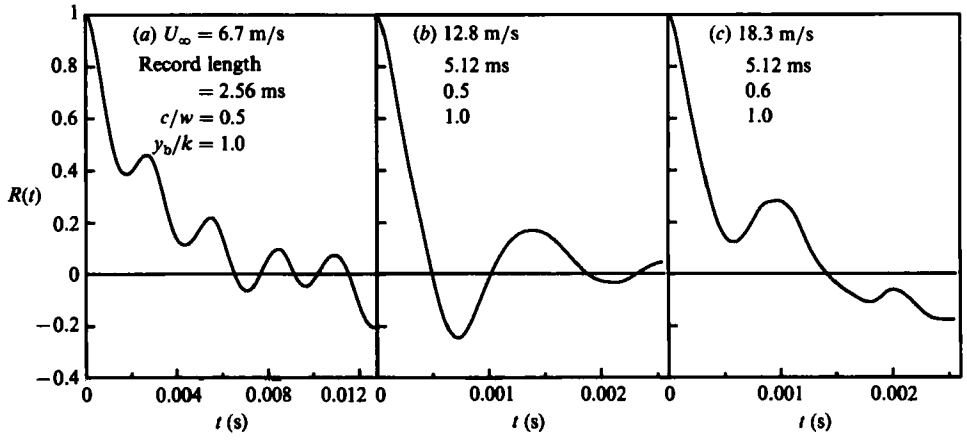

FIGURE 28. Distributions of short-time autocorrelation of velocity fluctuations in a k-type grooved wall; x = 66 cm.

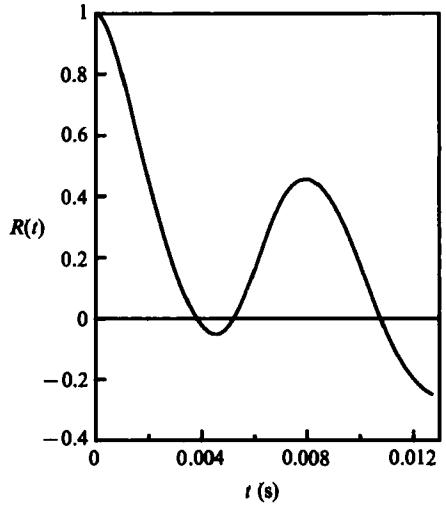

FIGURE 29. Short-time autocorrelation in a sandgrain-roughened wall; sandgrain size is grit 36; x = 66 cm; U_∞ = 4.9 m/s; record length = 25.6 ms; y_b/k = 1.0.

within the 'short time'. In this sense, the short-time autocorrelations were much like flow visualization when the sheddings can be individually observed. At each free-stream speed examined, 100 correlation distributions and T, the times to the first clear rerise therein, were stored in the computer.

(iii) *Histogram.* Figures 31–33, show examples of the histogram of the time period T. The histograms are skewed similar to the hydrogen-bubble-bursting data of Kim, Kline & Reynolds (1971). The standard deviation, σ is large – about $\frac{1}{3}$ of the mean time period $\overline{T}$; a similar observation has been made by Kim *et al.* from visual observations of the periodicity of bursting in a smooth wall.

(iv) *Long-time autocorrelation.* Several examples of the distribution of long-time autocorrelations of the velocity fluctuation signal in the rough walls are shown in figures 34–36. The time length of the record in 'long time' is 100 times larger than that in the previous 'short-time' data. In comparison to that in Kim *et al.*'s study

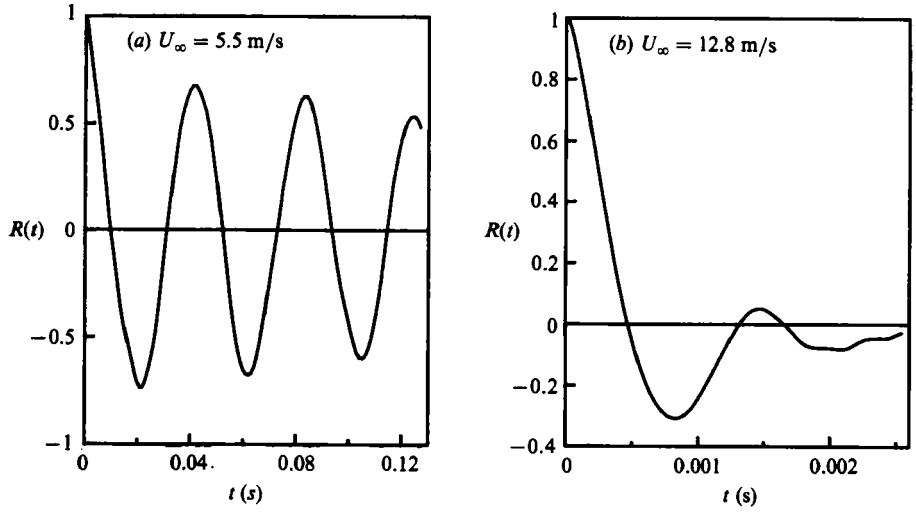

FIGURE 30. Short-time autocorrelation in a d-type grooved wall; $x = 66$ cm; $y_b/k = 1.0$; $c/w = 0.5$; (a) record length = 5.12 ms; (b) 12.8 ms.

on bursting in a smooth wall, the number of vortices shed in the rough walls during a 'long time' is several times higher. The mean values of the time period obtained from short-time autocorrelation are given in figures 34–36. The long-time autocorrelation has a tendency to rerise at these time intervals.

Although it is well accepted that the lower critical value of Re_k represents the onset of vortex shedding in a distributed roughness, there could be some question as to whether the structures going past the hot wire at the very lowest Reynolds numbers and particularly in the grooved walls can be truly described as vortices. *A priori*, the possibility cannot be ruled out that some of these structures could well be jets or even waves. In the present context, the exact nature of the structures does not seem to be crucial; the fact that a quasi-periodic phenomenon is in play justifies the study of its mean time period. After completing the present work, comparisons were made between the present measurements of $\overline{T}$ and those made recently by Klebanoff, Cleveland & Tidstrom (1987) behind isolated roughness elements (hemispheres and cylinders) in a laminar boundary layer. By simultaneous measurements using two hot wires, they have identified the shed structures to be vortices. In the present study, $\overline{T}$ is inversely proportional to $U_\infty^{1.64}$ in both the varieties of k-type wall and to U_∞^2 in the d-type wall. On the other hand, Klebanoff *et al.* have found that $\overline{T}$ is inversely proportional to U_∞^2. The similar values of the velocity exponent suggest that the structures involved in the present study may also be vortices.

8.2. *Strouhal-number variation with Reynolds number*

The Strouhal number St of vortex shedding in rough walls can be defined as

$$St = \frac{2\pi k}{\overline{T} U_\tau}, \tag{10}$$

where $\overline{T}$ is the mean time period of vortex shedding. The variation of St with Re_k is shown in figure 37. Combining figures 1 and 37, the relationship between drag and vortex shedding can be obtained.

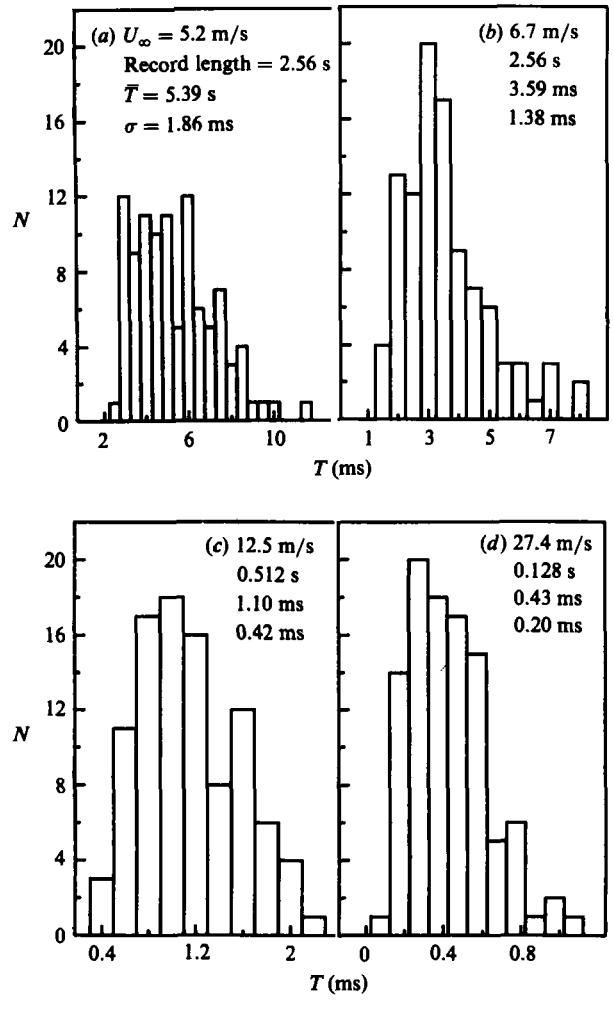

FIGURE 31. Histograms of time to first rerise in distributions of short-time autocorrelation of velocity fluctuations in a k-type grooved wall; $x = 66$ cm; $y_b/k = 1$; $c/w = 0.5$.

The measurements of Townes & Sabersky (1966) in square-grooved roughness, ranging in size from $\frac{1}{8}$ in. $\times \frac{1}{8}$ in. to 1 in. $\times$ 1 in., are included in figure 37. They measured the mean frequency $\bar{f}(= 2\pi/\bar{T})$ by flow visualization. Within the cavity, four typical flow phases were identified. These phases, termed 'strong exchange', 'weak exchange', 'inflow' and 'divide', appeared in random succession. They defined $\bar{f}$ as the mean frequency of phase change. The St versus Re_k relationship was found to be linear up to an Re_k of 150. For $Re_k > 150$, the cavity flow was qualitatively different; a 'well established, fairly steady vortex' occupied most of the cavity. The cavity flow at the downstream end was, however, found to 'flutter' and in this range of Re_k, $\bar{f}$ represents the mean rate of flutter. The Strouhal number was found to be constant and equal to 10 for $Re_k > 150$.

The best-fit linear relationships between St and Re_k, for the present data and those of Townes & Sabersky (1966), are shown in figure 37. The Strouhal numbers in the

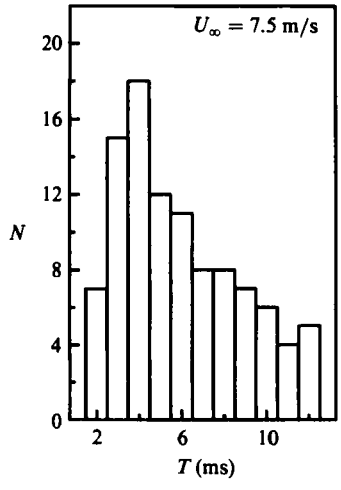

FIGURE 32.

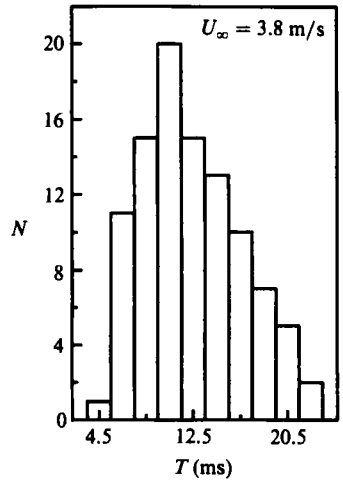

FIGURE 33.

FIGURE 32. A typical histogram of time to first rerise in distributions of short-time autocorrelation of velocity fluctuations in a d-type wall; $x = 66$ cm; $y_b/k = 1.2$; $c/w = 1.2$; total record length = 2.56 s; $\bar{T} = 6.01$ ms; $\sigma = 2.81$ ms.

FIGURE 33. A typical histogram of time to first rerise in distributions of short-time autocorrelation of velocity fluctuations in a sandgrain (grit 36)-roughened wall; $x = 66$ cm; record length = 5.12 s; $\bar{T} = 12.49$ s; $\sigma = 4.24$ s.

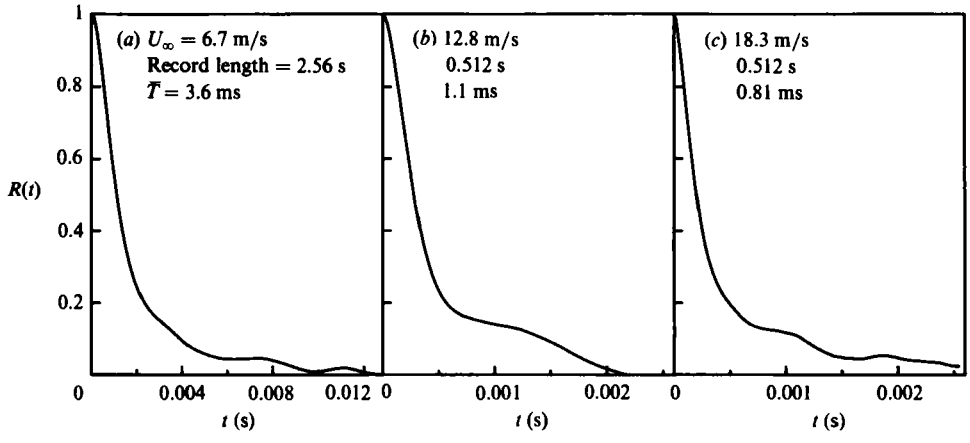

FIGURE 34. Distributions of long-time autocorrelation of velocity fluctuations in a k-type grooved wall; $x = 66$ cm; $y_b = k$; record length = 2.56 s.

present data are slightly higher. This may be due to the differences in the techniques of measurement. In the measurements of the time period between bursting in smooth-flat-plate boundary layers differences are known to exist depending on the technique of measurement. In any case, figure 37 shows the interesting result that the slope of the St versus Re_k line is about the same in the present data and in the work of Townes & Sabersky. Furthermore, this slope is independent of the geometry or type of the roughness element. The physical significance of the slope is that its square root $U_\tau(\bar{T}/\nu)^{\frac{1}{2}}$ can be described as a stability parameter (Black 1968). Note that it does not contain k. In the absence of a rigorous theoretical stability analysis,

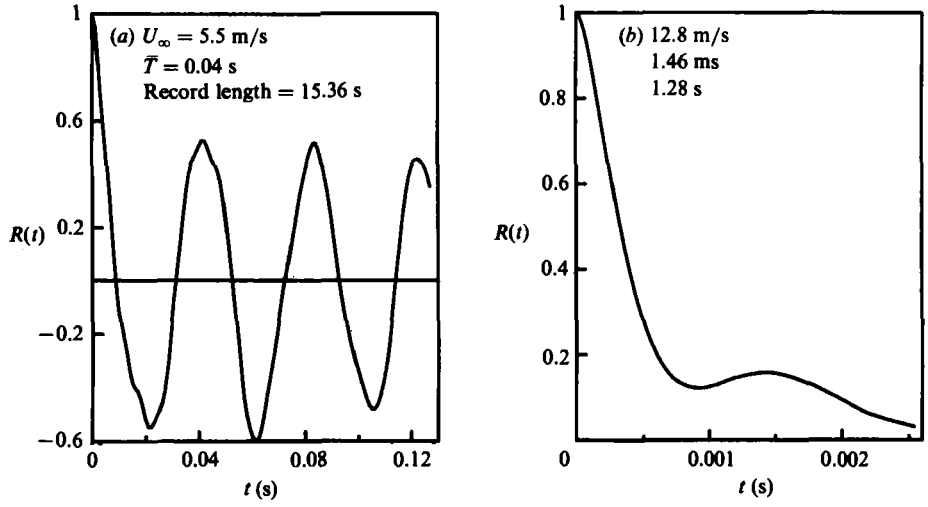

FIGURE 35. Distributions of long-time autocorrelation of velocity fluctuations in a d-type wall; $x = 66$ cm; $y_b/k = 1$, $c/w = 0.5$.

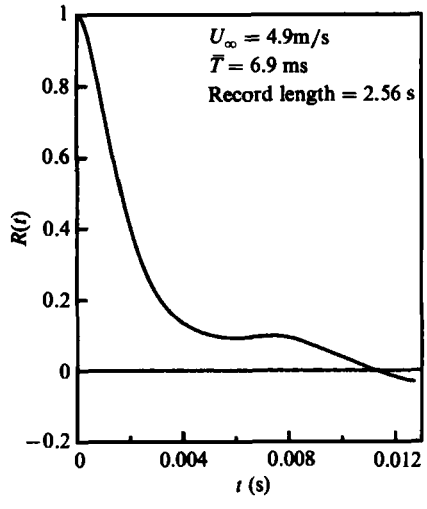

FIGURE 36. A typical distribution of long-time autocorrelation of velocity fluctuations in a sandgrain roughened (grit 36)-wall; $x = 66$ cm.

Black has shown empirically that the stability parameter in a smooth flat plate is determined by the two constants in the law of the wall, which implies that the parameter has a universal value. Black's theory envisages a periodic vortex train much as in the wake of a roughness element. Using the constants in (6), Black's theory yields a value of 10.5 for the parameter. A line with this slope is also shown in figure 37 to aid comparison. The absolute location of this line along the ordinate is not important. It is interesting to see that the value of Black's stability parameter agrees rather well with 10.0 in the data of Townes & Sabersky and 9.2 in the present data. The universal nature of the stability parameter may be related to the following: first, the structure of the boundary layer in rough and smooth walls is similar; secondly, the smooth-surface law of the wall applies to a rough wall also. The latter, although

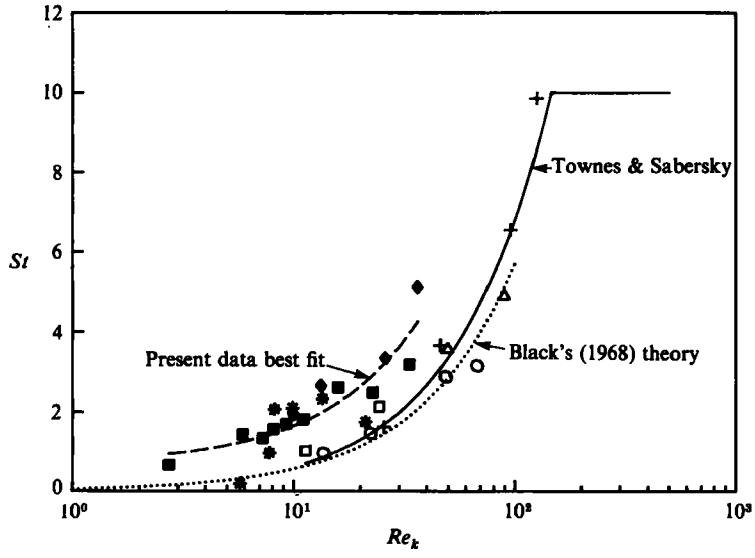

FIGURE 37. Universal nature of the stability parameter $U_\tau(\overline{T}/\nu)^{\frac{1}{2}}$. Present data: ■, k-type groove; *, d-type groove; ◆, Sandgrain grit 36. Townes & Sabersky (1966) d-type groove: □, $\frac{1}{8}$ in. × $\frac{1}{8}$ in.; ○, $\frac{1}{4}$ in. × $\frac{1}{4}$ in.; +, $\frac{1}{2}$ in. × $\frac{1}{2}$ in.; △, 1 in. × 1 in.

widely used, has never been independently established and the present results can be considered as a pointer in that direction.

9. Conclusions

The conclusions of the present investigation may be listed as follows.

(i) A self-preserving state can be reached in boundary layers developing over both d-type-groove and sandgrain roughnesses.

(ii) The method of velocity-profile matching can be used to estimate the local wall resistance in a zero-pressure-gradient rough-wall turbulent boundary layer having a low free-stream turbulence level.

(iii) The internal layer grows at the same rate no matter whether the step change in roughness is from smooth to d-type or smooth to k-type grooved wall.

(iv) In the k-type walls, the upper critical transition Reynolds number $(kU_\tau/\nu)_u$ determines the roughness function behaviour in both the transition and fully rough regime. The value of $(kU_\tau/\nu)_u$ drops with increasing aspect ratio of the roughness elements. The lower and upper critical Reynolds numbers correlate with the Reynolds numbers that indicate the onset and the development of irregularities respectively in the vortex shedding behind isolated roughness elements lying submerged in laminar boundary layers.

(v) The drag of a k-type rough wall can be reduced by lowering the spanwise aspect ratio of the roughness elements. The results would be noticeable below an aspect ratio of about 6 to 8.

(vi) The vortex shedding in rough-wall boundary layers is described by a constant value of the parameter $U_\tau(\overline{T}/\nu)^{\frac{1}{2}}$ irrespective of the type of roughness.

The author is indebted to National Aeronautics and Space Administration for financial support (NAS1-17296). He is also grateful for the interest shown by Mr D. M. Bushnell in the work, and to Mr R. D. Watson for assistance.

REFERENCES

ANTONIA, R. A. & LUXTON, R. E. 1971 The response of a turbulent boundary layer to a step change in surface roughness. Part 1. Smooth to rough. *J. Fluid Mech.* **48**, 721–761.

BANDYOPADHYAY, P. R. 1986 Drag reducing outer-layer devices in rough-wall turbulent boundary layers. *Exp. Fluids* **4**, 247–256.

BESSEM, J. M. & STEVENS, L. J. 1984 Cross-correlation measurements in a turbulent boundary layer above a rough wall. *Phys. Fluids* **27**, 2365–2366.

BETTERMANN, D. 1965 Contribution a l'etude de la couche limite turbulente le long de plaques rugueuses. *Rep.* 65-6, CNRS, Paris (in French).

BLACK, T. J. 1968 An analytical study of the measured wall pressure field under supersonic turbulent boundary layers. *NASA CR*-888.

CLAUSER, F. H. 1956 The turbulent boundary layer. *Adv. App. Mech.* **4**, 1–51.

COLEBROOK, C. F. & WHITE, C. M. 1937 Experiments with fluid motion in roughened pipes. *Proc. R. Soc. Lond.* A **161**, 367–381.

DVORAK, F. A. 1969 Calculation of turbulent boundary layers on rough surfaces in pressure gradient. *AIAA J.* **7**, 1752–1759.

FURUYA, Y. & MIYATA, M. 1972 Visual studies on the wake of a roughness element proximate to a wall. *Mem. Fac. Engng, Nagoya University* **24**, 278–293.

FURUYA, Y., MIYATA, M. & FUJITA, H. 1976 Turbulent boundary layer and flow resistance on plates roughened by wires. *ASME PAPER* 76-FE-6.

GLOTOV, G. F. & KORONTSVIT, IU. F. 1983 An investigation of a method for controlling a three-dimensional separation zone, *TsAGI. Uchenye Zapiski*, **14**, 126–131 (in Russian).

GOLDSTEIN, S. 1936 A note on roughness. *Aero. Res. Counc. R&M* 1763.

GRASS, A. J. 1971 Structural features of turbulent flow over smooth and rough boundaries. *J. Fluid Mech.* **50**, 233–255.

GÜVEN, O., FAREL, C. & PATEL, V. C. 1983 Boundary-layer development on a circular cylinder with ribs. *Trans. ASME* I: *J. Fluids Engng.* **105**, 179–184.

HAMA, F. R. 1954 Boundary layer characteristics for smooth and rough surfaces. *Trans. Soc. Naval Archit. Marine Engrs* **62**, 333–358.

HEAD, M. R. & BANDYOPADHYAY, P. 1981 New aspects of turbulent boundary-layer structure. *J. Fluid Mech.* **107**, 297–338.

KIM, H. T., KLINE, S. J. & REYNOLDS, W. C. 1971 The production of turbulence near a smooth wall in a turbulent boundary layer. *J. Fluid Mech.* **50**, 133–160.

KLEBANOFF, P. S., CLEVELAND, W. G. & TIDSTROM, K. D. 1987 On three-dimensional roughness and the evolution of a turbulent boundary layer. *AEDC TR*-87-7.

KLEIN, D. 1977 Pressure measurements and flow visualization over roughness elements. Ph.D. thesis, University of Missouri, Columbia.

MONIN, A. S. & YAGLOM, A. M. 1971 *Statistical Fluid Mechanics: Mechanics of Turbulence*, vol. 1. MIT Press.

MOORE, W. L. 1951 An experimental investigation of boundary layer development along a rough surface. Ph.D. thesis, State University of Iowa.

NIKURADSE, J. 1933 Strömungsgesetze in rouhen Rohren. *VDI Forchung.* No. 361 (*NACA TM*1292).

OSAKA, H., NISHINO, T., OYAMA, S. & KOGEYAMA, Y. 1982 Selfpreservation for a turbulent boundary layer over a *d*-type rough surface. *Mem. Fac. Engng, Yamaguch University* **33**, 9–16 (in Japanese).

PERRY, A. E. & JOUBERT, P. N. 1963 Rough wall boundary layers in adverse pressure gradients. *J. Fluid Mech.* **17**, 193–211.

PERRY, A. E., SCHOFIELD, W. H. & JOUBERT, P. N. 1969 Rough wall turbulent boundary layers. *J. Fluid Mech.* **37**, 383–413.

PRANDTL, L. & SCHLICHTING, H. 1934 Das Wiederstandagesetz rouher Platten. *Werft Reederer Hafen* **15**, 1–4.

PURTELL, L. P., KLEBANOFF, P. S. & BUCKLEY, F. T. 1981 Turbulent boundary layer at low Reynolds number. *Phys. Fluids* **24**, 802–811.

ROTTA, J. C. 1950 Das in Wandnähe gültige Geschwindigkeitsgesetz turbulenter Strömungen. *Ing.-Arch.* **18**, 277–280.

ROTTA, J. C. 1962 Turbulent boundary layers in incompressible flow. *Prog. Aero. Sci.* **2**, 1–219.

SCHILLER, L. 1932 Strömung in Rohren. *Handbuch der Experimentalphysik*, vol. 4, pp. 1–207.

SCHLICHTING, H. 1936 Experimentelle Untersuchungen zum Rauhigkeitsproblem. *Ing.-Arch. VII*, **1**, 1–34.

SCHLICHTING, H. 1979 *Boundary-Layer Theory*, 7th edn. McGraw-Hill.

SIMPSON, R. L. 1973 A generalized correlation of roughness density effects on the turbulent boundary layer. *AIAA J.* **11**, 242–244.

SMITH, A. M. O. & CLUTTER, D. W. 1959 The smallest height of roughness capable of affecting boundary-layer transition. *J. Aero. Sci.* **26**, 229–256.

TOWNES, H. W. & SABERSKY, R. H. 1966 Experiments on the flow over a rough surface. *Intl J. Heat Mass Transfer* **9**, 729–738.